MODELING OF TEMPERATURE IMPACTS ON FIXED FILM MICROBIAL GROWTH AND NITRIFICATION KINETICS

A Thesis
Submitted to the Graduate Facility
of the
North Dakota State University
of Agriculture and Applied Sciences

By

Jacob David Strombeck

In Partial Fulfillment of the Requirements
for the Degree of
MASTER OF SCIENCE

Major Department:
Civil Engineering

March 2014

Fargo, North Dakota

North Dakota State University
Graduate School

Title

Modeling of Temperature Impacts on Fixed Film Microbial Growth and Nitrification Kinetics

By

Jacob David Strombeck

The Supervisory Committee certifies that this ***disquisition*** complies with North Dakota State University's regulations and meets the accepted standards for the degree of

MASTER OF SCIENCE

SUPERVISORY COMMITTEE:

Dr. Wei Lin
Chair

Dr. Eakalak Khan

Dr. Peter Oduor

Dr. Bernhardt Saini-Eidukat

Approved:

March 10, 2014
Date

Dr. Dinesh Katti
Department Chair

ABSTRACT

Monod-type kinetic models, used in simulating microbial growth in biological treatment systems, suggest significant decreases of substrate utilization at lower temperatures. However, it is documented that performance of fixed film treatment systems are not hindered with declining temperatures. Previous studies at the Moorhead, MN, Wastewater Treatment Facility (WWTF) showed significant impacts of temperature on biofilm growth in its moving bed biofilm reactor (MBBR), and studies noted that at low temperatures more biomass was present. Previously, a series of kinetic bench-scale batch tests was performed to measure ammonium removal in the full-scale system. As part of this research, a diffusion based kinetic model was developed to simulate the bench-scale trials and determine if Monod kinetics and temperature corrections properly model fixed film systems. It was found that Monod kinetics and temperature corrections do apply to fixed film system as long as proper consideration is given to the change in biofilm characteristics.

TABLE OF CONTENTS

LIST OF TABLES

LIST OF FIGURES

LIST OF APPENDIX TABLES

CHAPTER 1. INTRODUCTION

It is widely understood that suspended growth biological wastewater treatment processes do not perform well in cold conditions. However, fixed film biological wastewater treatment processes are not plagued by performance decline due to cold water temperatures. This phenomenon has been observed by researchers and it is still poorly understood as to why temperature impacts are not very significant in fixed film systems. An example of a full-scale fixed film process experiencing this phenomenon is the City of Moorhead, Minnesota, Wastewater Treatment Facility (WWTF).

In an effort to reduce impairment of a portion of the Red River of the North, seasonal discharge ammonia-N limits were applied to the Moorhead WWTF. In order to meet these ammonia-N limits, the Moorhead WWTF began operation of a tertiary nitrification moving bed biofilm reactor (MBBR). Since operation began, the Moorhead MBBR has been capable of meeting the seasonal discharge limits, and contrary to design expectations, the Moorhead MBBR is capable of meeting the limits year round even with water temperature approaching 8.0 °C. Based on the ammonia-N removal rate percentage (Figure 1.1 and Figure 1.2), there is no indication that in winter months performance of the Moorhead MBBR was affected by the changes in the season and temperature. Ammonia-N removal rates greater than 70 percent and averaging higher than 90 percent have been sustained regardless of temperature.

Previous study efforts on the Moorhead MBBR observed seasonal changes in the biofilm thickness and biofilm surface area and affirmed that changes in the season and temperature result in significant changes in the amount of attached biomass. Additionally, a series of kinetic trials was performed in an effort to determine the impact of temperature on nitrification kinetics. A model was developed using the kinetic trial data that provided a good initial effort at modeling

MBBR fixed film nitrification kinetics; however, some questions remained to be answered (Bjornberg et al., 2010). As such, this research effort was undertaken to ultimately develop better kinetic models that incorporated the observed changes in attached biomass, changes in biofilm thickness, and changes in biofilm surface area.

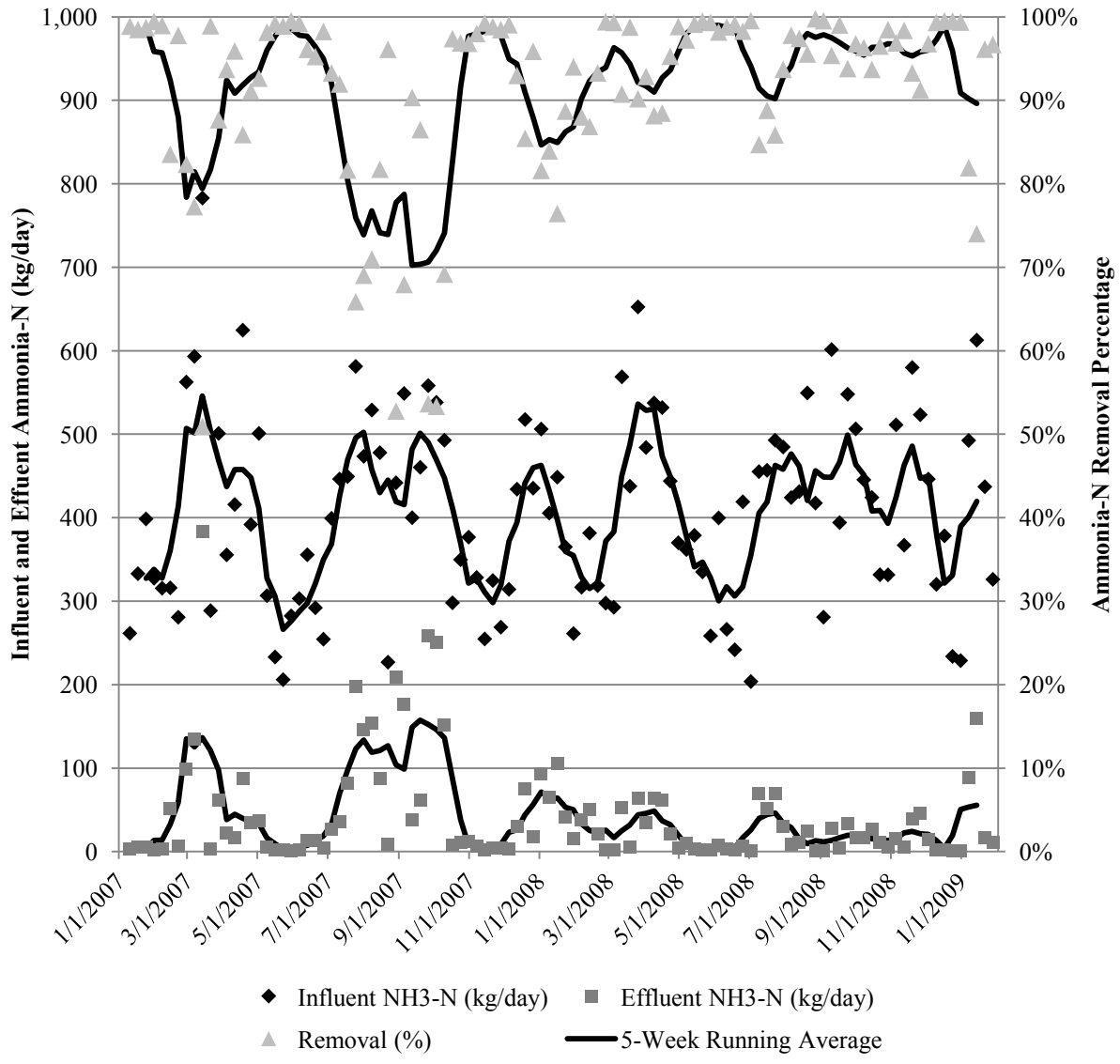

Figure 1.1. Weekly Moorhead MBBR historical influent and effluent ammonia-N loading rate (kg/d) and ammonia-N removal percentage (Source: Bjornberg et al., 2010)

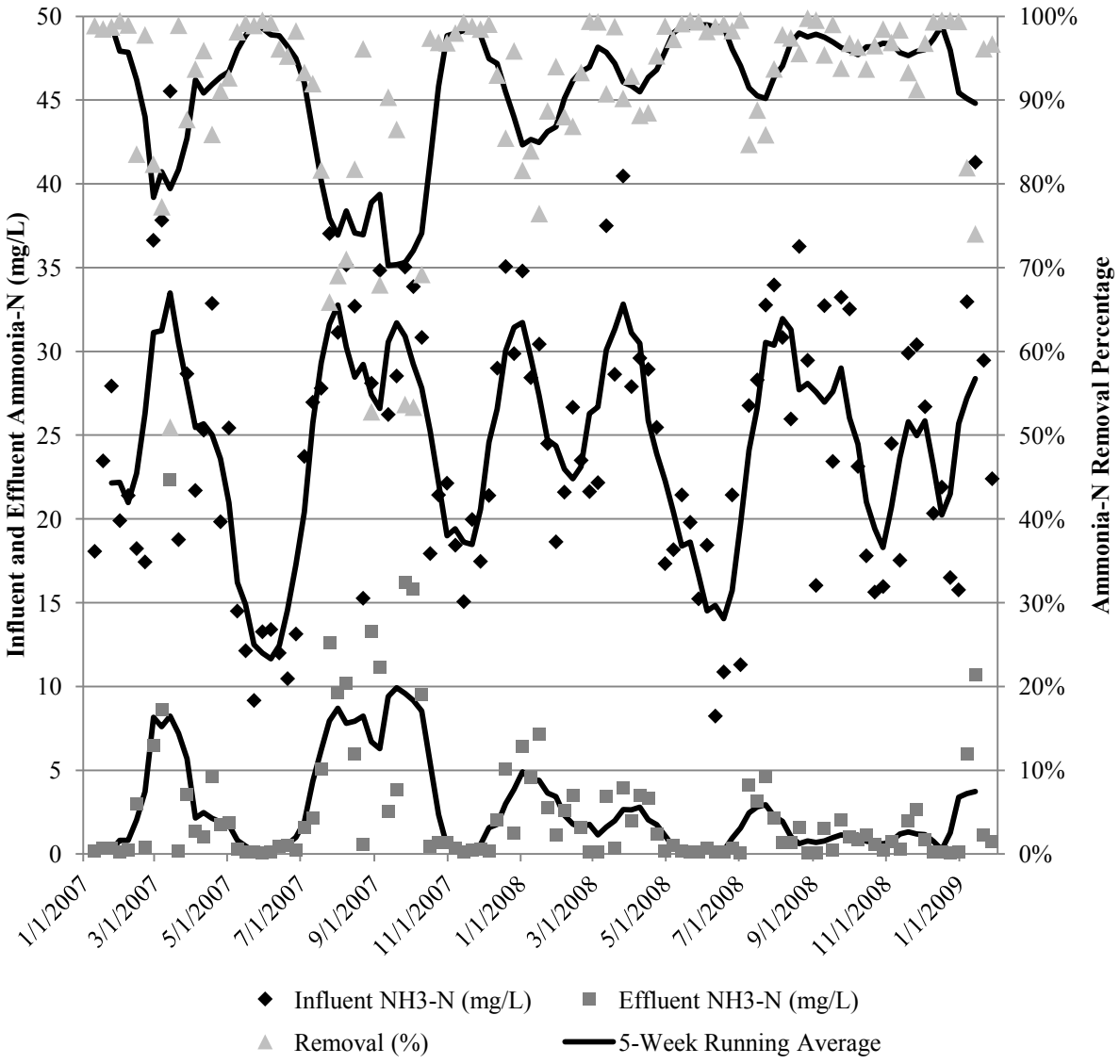

Figure 1.2. Weekly Moorhead MBBR historical influent and effluent ammonia-N concentration (mg/L) and ammonia-N removal percentage (Source: Bjornberg et al., 2010)

The primary objective of this study is better understanding of how changes in water temperature affect nitrification kinetics and overall performance of full-scale fixed film wastewater treatment processes by utilizing data and information from the Moorhead MBBR. The specific goals of this study include:

1. Evaluation of how biofilm characteristics (biomass per unit area, biomass thickness, biofilm surface area, and biomass density) change with temperature;
2. Development of a diffusion based unsteady-state model using Monod kinetics, and use of the model to simulate nitrification using bench-scale trial data with consideration to changes in biofilm characteristics as a result of temperature changes; and
3. Use of the biofilm characteristics and results of the unsteady-state model to determine the temperature impacts to Monod kinetic parameters.

Background information, methodology and model development, and results and discussions for this study are contained in subsequent chapters. Background on fixed film processes, nitrification, nitrification kinetics, and modeling of fixed film processes is provided in Chapter 2. A summary of the Moorhead MBBR and information regarding previous Moorhead MBBR research efforts is incorporated into Chapter 3. Description of the methodology, model development, and procedure for solving the model are included in Chapter 4. Results and discussions and ideas for furthering this research topic incorporated in Chapter 5.

CHAPTER 2. LITERATURE REVIEW

Background information related to this research effort is presented in this chapter and it explores the latest understanding of fixed film wastewater treatment processes, the nitrification process and kinetics, and the state of practice for modeling fixed film treatment systems. Background relating to the Moorhead WWTF and their ammonia treatment strategy and recent research efforts undertaken regarding the facility is also presented in this chapter.

2.1. Fixed Film Microbial Growth and Wastewater Treatment Applications

Biological wastewater treatment usually occurs after primary wastewater treatment which generally consists of screening and sedimentation. Biological wastewater treatment processes are used for carbonaceous biological oxygen demand (CBOD) removal, typically referred to as secondary treatment, and are used for a variety of post-secondary treatment including nitrification, denitrification, and phosphorus removal. Biological wastewater treatment processes can be grouped into four broad categories: (1) suspended growth systems; (2) attached growth (fixed film) systems; (3) combined (hybrid) suspended and attached growth systems; and (4) lagoon systems. Depending on the system configuration and operating conditions, all biological wastewater treatment processes are capable of performing secondary and post-secondary treatment, with the exception of lagoon systems, which can only achieve limited post-secondary treatment (Metcalf & Eddy, 2003).

Fixed film biological treatment processes are defined as processes where the microorganisms responsible for the removal of target pollutants are attached to an inert material. This is opposed to the suspended growth systems where the microorganisms are maintained in liquid suspension. There are many different fixed film systems used in wastewater treatment,

including trickling filters, rotating biological contactors, fixed media submerged biofilters, granular media biofilters, and fluidized bed reactors (Rusten et al., 2006). Two additional treatment processes are gaining in popularity; the moving bed biofilm reactor (MBBR) process (Rusten et al., 2006) and the integrated fixed film activated sludge (IFAS) process (Regmi et al., 2011). These types of fixed film processes are gaining popularity because of their ease of implementation and retrofitting due to smaller footprints than more conventional processes and their ease of operation (Regmi et al., 2011).

The MBBR system was developed by Kaldnes Milijøteknologi in the late 1980s and early 1990s, with the intent to combine the best features of an activated sludge system and a submerged biofilter system. MBBR systems are gaining in popularity and are being utilized for BOD removal and/or nitrification in wastewater treatment. The MBBR systems rely on numerous free-floating plastic media to provide a protected surface for the microorganisms to grow. The systems are designed to rely solely on the attached biomass and contribution to wastewater treatment by suspended growth is negligible. For this reason, sludge recycle is not required (Rusten et al., 2006). The plastic media of various sizes and shapes, provides 200 to 500 m^2/m^3 of protected surface area, are commonly used to fill 25 to 50 percent of the reactor volume (Metcalf & Eddy, 2003). MBBR systems can be designed for aerobic, anoxic, or anaerobic applications. When operating in aerobic mode, the reactor is mixed and media kept moving by a course bubble aeration system; when operating in anoxic or anaerobic conditions, mixing is achieved via mechanical mixers (Rusten et al., 2006).

The IFAS process is a similar process to the MBBR system; however, it is considered to be a hybrid process relying on both fixed film and suspended growth microorganisms. The same types of plastic media used in MBBR systems are commonly utilized in IFAS systems. The key

difference from a MBBR system is that a mixed liquor suspended solids is maintained and sludge recycle is required; providing for an advantageous strategy for a combined BOD removal and nitrification (Regmi et al., 2011). The design process for and operation of an IFAS system is more complicated than for a MBBR system (Zimmerman et al., 2005).

Modeling for microbial growth wastewater treatment systems varies between targeted removal parameters, system types, and operating conditions. Fixed film microbial growth kinetics, specifically related to nitrification, is presented in Section 2.3 and modeling techniques for fixed film systems are presented in Section 2.4.

2.2. Nitrification

Nitrogen is an important element in water bodies and is needed for the growth of microorganisms, phytoplankton, and plants. Nitrogen is used for amino acid production, protein synthesis, cell growth, and energy transfer. The nitrogen cycle is very complex and many natural sources of nitrogen exist with the largest source being atmospheric fixation (WEF, 1998). Other natural sources include precipitation, biological decomposition, and animal excretion. Additionally, there are many man-made sources of nitrogen in aquatic environment, with some of the largest contributors being urban and agricultural runoff, industrial discharges, petroleum and food processing plants, and domestic wastewater. Increased nitrogen in aquatic environments can have negative impact and result in toxicity to aquatic life, dissolved oxygen (DO) consumption, and eutrophication (Metcalf & Eddy, 2003).

The primary forms of nitrogen found in aquatic environments include organic nitrogen, ammonia, nitrite, and nitrate. However, nitrite and nitrate are not commonly found in raw domestic wastewater because free oxygen is not typically present to promote the oxidation to

other nitrogen forms. Total Kjeldahl Nitrogen (TKN) is the sum of the organic nitrogen and ammonia and is typically used as a measurement of the nitrogen content of raw domestic wastewater (WEF, 1998).

Ammonia represents approximately 60 percent of the TKN in domestic wastewater with the primary sources being the conversion of organic nitrogen into ammonia through the deamination of proteins and the hydrolysis of urea (WEF, 1998). Without treating wastewater for ammonia, discharge of domestic wastewater represents a significant increase in ammonia concentrations in water bodies which, as previously mentioned, can lead to toxicity to aquatic life, DO consumption, and eutrophication.

Ammonia exists in aqueous environments in two forms depending on the pH: as the ammonium ion (NH_4^+) or as free ammonia (NH_3). Typically, laboratory experiments consider the ammonia concentration to be the sum of both the ammonium ion and free ammonia concentration and report the concentration as ammonia as nitrogen (ammonia-N or NH_3-N) (Metcalf & Eddy, 2003). Reporting concentrations of nitrogen species as nitrogen and referring to ammonia nitrogen as the sum of both the ammonium ion and free ammonia species will be the standard herein.

Nitrification is the biological oxidation of ammonia to nitrite (NO_2^-), which is then further oxidized to nitrate (NO_3^-). The process is performed by autotrophic bacteria, which gain energy by the oxidation of ammonia or nitrite and are slower growing organisms than heterotrophic bacteria. Nitrification is a two-step process: *Nitrosomonas* bacteria first oxidize ammonia into nitrite, and then *Nitrobacter* bacteria oxidize nitrite into nitrate. There are other forms of autotrophic bacteria that are capable of performing nitrification; however, *Nitrosomonas* and *Nitrobacter* bacteria are primarily responsible for the process. The following

chemical equations govern the reduction of ammonia during the nitrification process, where *Nitrosomonas* bacteria perform Equation 2.1 and *Nitrobacter* bacteria perform Equation 2.2 (WEF, 1998). The chemical equation for the complete nitrification process is shown as Equation 2.3. Based on this stoichiometry, it requires 3.43 g of oxygen to nitrify 1.0 g of ammonia-N to nitrite and 4.57 g of oxygen to nitrify 1.0 g of ammonia-N to nitrate.

$$NH_4^+ + 1.5O_2 \rightarrow NO_2^- + 2H^+ + H_2O \quad (2.1)$$

$$NO_2^- + 0.5O_2 \rightarrow NO_3^- \quad (2.2)$$

$$NH_4^+ + 2O_2 \rightarrow NO_3^- + 2H^+ + H_2O \quad (2.3)$$

However, Equations 2.1 through 2.3 do not account for nitrogen uptake and utilization by the nitrifying bacteria. Considering that the microbial cells can be represented by the chemical formula $C_5H_7O_2N$, Equation 2.4, can be used represent the complete oxidation reduction of ammonia (Biesterfeld et al., 2001). From this equation, it is evident that alkalinity, commonly reported as calcium carbonate ($CaCO_3$), is required by the nitrifying bacteria to perform nitrification. Based on this stoichiometry, it requires 4.32 g of oxygen to nitrify 1.0 g of ammonia-N to nitrate; 0.25 g of oxygen less than required of the oxidation reduction alone (Equation 2.3). Theoretically, the process also requires 7.07 g of alkalinity as $CaCO_3$ per g of ammonia-N, with actual nitrification processes being measured between 6.0 and 7.4 g of alkalinity as $CaCO_3$ per g of ammonia-N oxidized to nitrate (Biesterfeld et al., 2001). The stoichiometry also indicates that a theoretical yield of 0.13 g of nitrifying biomass is generated during the destruction of 1.0 g of ammonia-N.

$$NH_4^+ + 1.89O_2 + 0.0805CO_2 \rightarrow 0.0161C_5H_7O_2N + 0.984NO_3^- + 1.98H^+ + 0.952H_2O \quad (2.4)$$

In summary, the primary goal of nitrifying wastewater prior to discharge is to prevent the nitrification process from occurring naturally in water bodies resulting in lowered DO concentrations and other negative impacts. Typically referred to as nitrogenous oxygen demand (NOD), the excess ammonia in water bodies can significantly lower DO concentrations and lead to eutrophication. The NOD of a receiving water body is further increased under the right stream flow conditions, with lack of sufficient reaeration, and due to the presence of large populations of nitrifying bacteria (WEF, 1998).

2.3. Nitrification Kinetics and Temperature Impacts

A handful of microbial growth models are commonly used, and it is important to note that all kinetic expressions for biomass growth and substrate utilization are empirical in nature and based on experimentally determined coefficients. For applications where the limiting substrate(s) are in dissolved form, it is most common to use Monod kinetics to model microbial growth and substrate utilization including the nitrification process (Metcalf & Eddy, 2003).

Monod kinetics, as shown in Equations 2.5 and 2.6 for nitrification, are a set of coupled equations that model the change in biomass concentration (dX/dt) as well as the change in ammonia-N concentration (dN/dt) due to biological uptake and degradation. The biomass growth and substrate utilization are functions of ammonia-N concentration (N), the biomass concentration (X), the ammonia-N half-saturation concentration (K_N), and a maximum specific growth rate (μ_m) of the biomass. The half-saturation concentration is the substrate concentration at which the specific growth rate is equal to half of the maximum growth rate. The biomass

growth equation includes an endogenous decay coefficient (k_d) to account for microbial respiration and death. The substrate utilization equation incorporates a biomass yield coefficient (Y) that relates the amount of microbial growth to the amount of ammonia-N required to achieve the growth. An additional expression that is commonly used is the maximum specific utilization rate (k) is shown as Equation 2.7 and is simply the ratio between μ_m and Y.

$$\frac{dX}{dt} = \frac{\mu_m N}{K_N + N} X - k_d X \tag{2.5}$$

$$\frac{dN}{dt} = -\frac{\mu_m N}{K_N + N} \frac{X}{Y} \tag{2.6}$$

X = biomass concentration (g/m^3)

t = time (days)

μ_m = maximum specific growth rate (d^{-1})

N = ammonia-N concentration (g/m^3)

K_N = ammonia-N half-saturation concentration (g/m^3)

k_d = endogenous decay coefficient (g biomass / g biomass / d)

Y = yield coefficient (g biomass / g substrate utilized)

$$k = \frac{\mu_m}{Y} \tag{2.7}$$

k = ammonia-N maximum specific utilization rate (g / g biomass / d)

The biomass concentration (X) for the nitrification process is commonly considered to involve ammonia oxidizing bacteria (AOB) and nitrite oxidizing bacteria (NOB). Ammonia

oxidation by AOB is usually the rate-limiting step in nitrification (Chen et al., 2006). Therefore, modeling only the AOB process and ammonia removal can successfully model the nitrification process.

The biomass concentration (X) for suspended growth systems is typically expressed as total suspended solids (TSS) with units of mg-TSS/L, as volatile suspended solids (VSS) with units of mg-VSS/L, or in terms of chemical oxygen demand (COD) with unit of mg-COD/L. VSS and COD are more common because they are better indicators of the presence of organics such as nitrifying bacteria. A common conversion between these units is 1.42 g-COD/g-VSS, which is based on assuming the microbial cells can be represented by the chemical formula $C_5H_7O_2N$ (Metcalf & Eddy, 2003). Conversions between TSS units are tougher and require knowledge of the biomass fraction that is organic. Assuming that the biomass has a 15 percent ash content, the theoretical conversion is 1.20 g-COD/g-TSS (Grady et al., 2011). The same conversions apply in fixed film systems except biomass concentration is commonly referred to a biomass density and the units are in terms of total solids (TS) and volatile solids (VS). In typical wastewater treatment fixed film applications the biomass density, in terms of TS, ranges from 10 to 60 kg/m^3 but can be as high as 200 kg/m^3 (Henze et al., 2008).

Several sources were reviewed to analyze Monod kinetic parameters that have been determined for nitrification. The sources include reference textbooks and research papers that discussed nitrification modeling efforts. A summary of the reference Monod kinetic parameters from modeling effort that had calculated most of the kinetic parameters is shown in Table 2.1. The units for the yield coefficients in the table were converted to volatile solids units following the biomass conversions previously mentioned. Additionally, many modelers assume an ammonia-N half-saturation concentration (K_N) of 0.5 to 1.0 mg/L (Grady et al., 2011).

Table 2.1. Nitrification Monod kinetic parameters

μ_m day^{-1}	Y mg/mg[a]	K_N mg/L[b]	k_d day^{-1}	Temp °C	System Type[c]	Source
Reference						
0.200 – 0.900	0.100 – 0.150	0.50 – 1.00	0.050 – 0.150	20	SG & FF	[1]
0.336 – 2.208	0.042 – 0.246	0.06 – 5.60	0.005 – 0.168	20	SG & FF	[2]
Modeling Efforts						
0.391	0.239	5.14	0.021	--	SG	[3]
0.696	0.183	1.21	0.050	25 – 26	FF	[4]
0.430	0.050	1.00	0.023	12	SG & FF	[5]
0.500	0.169	--	0.150	15	FF	[6]
0.420	0.330	0.27	0.040	35 – 37	SG	[7]
0.090	0.169	0.90	0.100	20	SG	[8]

[a] Yield coefficient (Y) units are expressed as mg-VS/mg-N or mg-VSS/mg-N

[b] Half-saturation concentration (K_N) units expressed as mg/L as ammonia-N

[c] System types are generalized and include suspended growth (SG) or fixed film (FF)

[1] Metcalf & Eddy, 2003

[2] Grady et al., 2011

[3] Dinçer & Kargı, 2000

[4] Lin, 2008

[5] Sen & Randall, 2008

[6] Sin et al., 2008

[7] Thalla et al., 2010

[8] Katipoglu-Yazan et al., 2012

A study of full-scale fixed film nitrification using rotating biological contactors found that nitrifying biofilms have a higher VS/TS ratio than heterotrophic biofilms. The nitrifying biofilms had a volatile solids to total solids ratio (VS/TS) of 82.5 to 90.3 percent with an average of 88.2 percent as compared to 66.6 to 82.3 percent with an average of 73.4 percent for heterotrophic biofilms (Meng & Ganczarczyk, 2004). The measured VS/TS ratio for nitrifying biofilms is very close to the 15 percent ash content assumed above. However, lower nitrifying TS/VS ratios have been reported for MBBR systems. A VS/TS range of 0.246 to 0.341 was

reported by Zhang et al. (2013) claiming that the low VS/TS ratios were because the system was treating raw water with oligotrophic conditions.

Another study analyzed nitrifying biomass to determine biomass AOB and NOB components. It was found that the AOB occupied 21.1 (±2.6) percent of the total biomass and increased to 31.6 (± 4.2) percent as the ammonia loading was increased from 0.013 (± 0.017) g/m^2-d to 0.236 (± 0.021) g/m^2-d as ammonia-N. Likewise the NOB occupied 15.8 (± 2.0) percent of the total biomass and increased to 20.8 (± 2.2) percent during the same increased loading. The remaining biofilm consisted of other bacteria and inert solids. With a further loading rate increase to 4.54 (± 0.99) g/m^2-d as ammonia-N, the nitrifying bacteria population was allowed to flourish and occupied roughly 75 percent of the biomass (AOB: 46.2 ± 5.2 percent, NOB: 28.8 ± 2.6 percent) (Zhang et al., 2013). Other modelers have accounted for the split between AOB and NOB by assuming 50 percent of the nitrifying biomass (50 percent of the VS) consisted of AOB and the other 50 percent consisted of NOB (Seifi & Fazaelipoor, 2012).

The Monod parameters that describe the kinetic rate are the maximum specific growth rates (μ_m), the half-saturation concentration (K_N), the endogenous decay coefficient (k_d), and the yield coefficient (Y). It is commonly understood that these parameters are affected by the wastewater temperature. The yield coefficient tends to have minimal temperature impacts and most researchers assume the temperature impacts on the yield to be negligible. Additionally, for autotrophic bacteria, there is no consensus among researchers to the temperature impacts on the half-saturation coefficient and many researchers assume a constant value (Grady et al., 2011).

Nevertheless, it is common to model temperature impacts on Monod kinetic parameters using an Arrhenius-type relationship (Equation 2.8). This equation correlates the kinetic parameters values (K_{T1}) at one temperature (T_1) to the kinetic parameters values (K_{T2}) at another

temperature (T_2) using a temperature-activity coefficient (θ_k). It is generally assumed that the endogenous decay coefficient (k_d) has a similar temperature-activity coefficient to the maximum specific growth rate (μ_m) (Metcalf & Eddy, 2003). Typical reference textbook values along with values determined from other fixed film modeling efforts for the temperature-activity coefficient ($\theta\mu$) for the maximum specific growth rate are shown in Table 2.2. The temperature-activity coefficients for the endogenous decay coefficient (k_d) are likely similar.

$$K_{T2} = K_{T1} \times \theta_K^{T2-T1} \quad (2.8)$$

K_{T1} = kinetic parameter at T1 °C (d^{-1})

K_{T2} = kinetic parameter at T2 °C (d^{-1})

θ_K = temperature-activity coefficient for parameter k

Table 2.2. Nitrification temperature-activity coefficients for μ_m (and approximately for k_d)

Temperature-Activity Coefficient	System Type	Source
Reference		
1.076 – 1.123	--	WEF, 1998
1.060 – 1.123	--	Metcalf & Eddy, 2003
1.068 – 1.118	--	Grady et al., 2011
Fixed Film Modeling Efforts		
1.090	Full-Scale	Rusten et al., 2006
1.072	Pilot-Scale	Houweling et al., 2007
1.103	Pilot-Scale	Sin et al., 2008
1.111	Full-Scale and Pilot-Scale	Boltz et al., 2009
1.099	Pilot-Scale	Zhang et al., 2014

However, as noted in Chapter 1, the temperature impacts on nitrification for fixed film systems are not very well understood. Even though the kinetic rates may change, overall performance does not diminish at colder temperatures. It should also be noted that some of the information provided in Table 2.2 is based on results from pilot-scale efforts and more research related to operational full-scale systems is needed. A recent study indicates that, under nitrogen limiting conditions, the effect of temperature on the nitrification performance in a fixed film process is greatly reduced when compared to suspended growth systems (Zhu & Chen, 2002). Furthermore, it was noted that substrate diffusion, mass transport, and other phenomena impacts the effect of temperature on nitrification kinetics for fixed film systems, and that the impact of temperature on nitrification is less pronounced than it is for suspended growth systems (Chen et al., 2006). An additional study found that under ammonia limiting conditions the apparent temperature impacts to the overall nitrification rate was negligible between the temperature of 10.2 and 23.3 °C (Salvetti et al., 2006). In a more recent study, it indicated that a 98.2 percent ammonia-N removal rate was achieved at 18.4 °C and an 82.0 percent ammonia-N removal was still achieved at 11.1 °C; however, only an average ammonia-N removal rate of 16.0 percent was observed at lower temperature around 3.7 °C. The same study concluded that nitrification performance is not greatly impacted by temperature until the temperature drops below 5.0 °C (Zhang et al., 2013). This same apparent lack of temperature impacts to the nitrification rate has been observed in the nitrifying MBBR at the Moorhead WWTF (Bjornberg et al., 2010).

In a slightly different temperature impact to nitrification study, an analysis of the AOB and NOB biomass fractions was performed. It was found that the AOB and NOB are only limitedly impacted by temperature, and rather the percentages of nitrifiers in the biomass were impacted by the ammonia-N loading rate. Larger ammonia-N loading rates resulted in an

increase in both the AOB and NOB fractions of the total biomass (Zhang et al., 2013). Based on this observation, the ammonia-N loading rate can influence the biomass development, specifically the percentage of the biomass occupied by AOB and NOB.

DO concentration, pH, and alkalinity can affect the nitrification rate. A DO concentration of 1.0 to 2.0 mg/L is roughly the minimum DO concentration required to not limit AOB growth, and a slightly higher minimum range of 2.0 to 4.0 mg/L is required to not limit the NOB growth (Chen et al., 2006). Because of different oxygen requirements for AOB and NOB, it is possible to design nitrification systems that only oxidize ammonia to nitrite and not complete the nitrite oxidation to nitrate. As for pH, there is much disagreement as to the impacts on the nitrification process. A wide range of optimum pH ranges have been reported and indicate a pH range of 7.0 to 8.8 being optimum (Chen et al., 2006). As previously indicated, alkalinity is required for nitrification and to help maintain pH in the reactor. An insufficient alkalinity will allow the nitrification process to reduce the pH and lower the nitrification rate. For fixed film systems with thin biofilms (less than approximately 100 μm thick), maximum nitrification rates were still observed at alkalinity concentrations as low as 70 mg/L as $CaCO_3$, and higher alkalinity concentrations are required for thick biofilms (Rusten et al., 2006).

2.4. Fixed Film (Biofilm) Modeling

Biofilms are non-uniform agglomerations of bacteria and higher order organisms held together and attached to the media with extracellular polymeric substance (EPS). Microbial cells have the intrinsic ability to assemble these integrated biofilm communities when a material on which to attach is present. A conceptualization of the biofilm system, which includes the attachment support, the biofilm (base film and surface film), the bulk liquid, and in some cases a

gas phase, is presented as Figure 2.1. If present, mass transport through the gas phase and into the bulk liquid is governed by the substrate's solubility and modeled with Henry's Law. Mass transport in the biofilm is controlled by diffusion, while mass transport through the surface film between the bulk liquid and the biofilm is governed by advection and turbulent diffusion. The shape of the biofilm and thickness of the surface film is largely dependent on the hydrodynamic flow regime of the system (Grady et al., 2011).

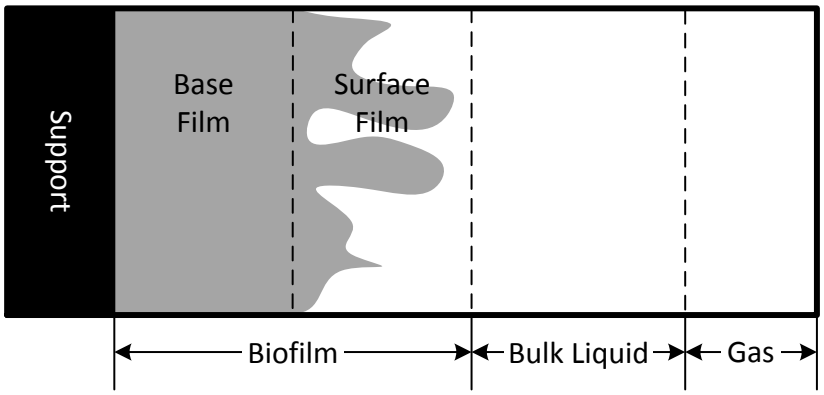

Figure 2.1. Conceptualization of a biofilm system (Source: Grady et al., 2011)

The primary method for modeling fixed film systems is diffusion based modeling with geometric simplifications of the biofilm. The most common method involves simplifying the biofilm geometry, assuming a flat biofilm surface, and assuming a hypothetical liquid layer separates the biofilm from the bulk liquid, as shown in Figure 2.2. This modeling approach can be used to model nitrification for fixed film processes, where the limiting substrate becomes ammonia-N (Grady, Daigger, Love, & Filipe, 2011).

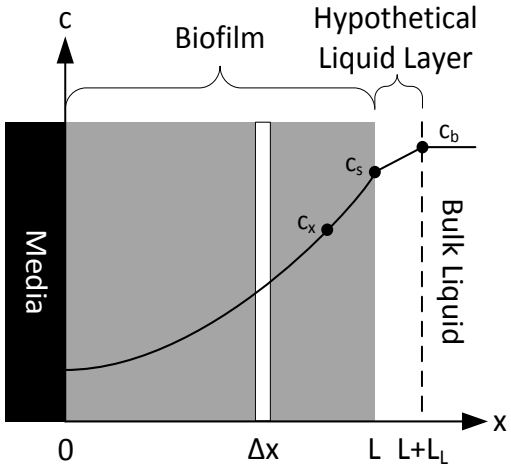

Figure 2.2. Conceptual biofilm with ideal concentration profile (Source: Grady et al., 2011)

The substrate flux (J_c) out of the bulk liquid and into the biofilm is modeled by implementing a hypothetical stagnant liquid layer immediately outside of the biofilm with substrate concentration c_b equating to the bulk concentration and c_s corresponding to the concentration at the surface of the biofilm (Grady et al., 2011). At the interface between the hypothetical stagnant liquid layer and the biofilm, the substrate flux (J_c) across the hypothetical stagnant liquid layer is equal to the flux into the biofilm. This flux is approximated by multiplying the difference in substrate concentration on either side of the stagnant liquid layer by the substrate diffusion coefficient in water (D_W) divided by the thickness of the stagnant liquid layer (L_L). This relationship is shown as Equation 2.9.

$$J_c = \frac{D_W}{L_L}(c_b - c_s) \tag{2.9}$$

J_c = unit substrate flux (g/m^2-d)

D_W = substrate diffusion coefficient in water (m^2/d)

L_L = thickness of stagnant liquid layer (m)

c_b = bulk liquid substrate concentration (g/m^3)

c_s = substrate concentration at liquid-biofilm interface (g/m^3)

The substrate diffusion coefficient in water (D_W) and the liquid layer thickness (L_L) describe the mass transport within the hypothetical liquid layer. The diffusion coefficient for ammonia in water is temperature dependent and ranges from 1.10×10^{-4} m^2/d at 10 °C to 1.49×10^{-4} m^2/d at 20 °C (Stewert, 2003). The liquid layer thickness is dependent of flow regime and is thicker for systems experiencing laminar flow conditions resulting in more resistance to mass transfer, and the liquid layer thickness will be thinner under turbulent conditions. A value of 40 μm was used for a completely-mixed biofilm nitrification system under turbulent conditions (Thalla et al., 2010).

Fick's first law of diffusion, as shown in Equation 2.10, is commonly used to model the substrate flux (J_c) in the biofilm. Fick's first law relates the substrate flux (J_c) to an effective substrate diffusion coefficient (D_B) multiplied by the concentration gradient (dc/dx) within the biofilm. The effective diffusion coefficient (D_B) is usually smaller than the diffusion coefficient in water (D_W) because the effective diffusion coefficient takes into account more than just molecular diffusion and incudes considerations for channels and diffusional pathways within the biofilm (Grady et al., 2011). Smaller effective diffusion coefficients indicate an increased resistance to mass transport and an increased diffusional length.

$$J_c = -D_B \frac{dc}{dx} \tag{2.10}$$

D_B = effective substrate diffusion coefficient in the biofilm (m^2/d)

c = substrate concentration (g/m^3)

x = distance into biofilm (m)

The effective diffusion coefficient is dependent on the biomass density (more dense results in smaller coefficients) and the molecular weight of the substrate (larger weights results in smaller coefficients), with the ratio of the effective diffusion coefficient to the diffusion coefficient in water (D_B/D_w) between 0.5 and 0.8 for ammonia (Stewert, 2003). The flow regime can also be a factor for determining the effective diffusion coefficient, especially when modeling without the stagnant liquid layer. For example, D_B/D_w ratios between 0.32 and 0.70 have been used to model denitrification biofilms under laminar flow conditions (Melo, 2005). Many nitrification researches modeling IFAS or MBBR systems use a D_B/D_w ratio of 0.8 in biofilms (Lin, 2008; Boltz et al., 2009; Göransson, 2004).

The actual biofilm is modeled by performing a mass balance around a control volume within the biofilm (as shown in Figure 2.2), where the change in mass of substrate with time ($\dot{M}$) is equal to the control volume (ΔV) multiplied by the change in substrate concentration with respect to time ($\partial c/\partial t$). Using Fick's first law with the effective substrate diffusion coefficient (D_B), the substrate mass transport into and out of the control volume can be taken as the flux (J_c) multiplied by the cross-sectional area (A). The substrate utilization with the biofilm is modeled using Monod kinetics. The control volume mass-balance is shown in Figure 2.2 and as Equation 2.11, where Fick's first law has been substituted into for the flux terms (J_c).

$$\dot{M} = \Delta V \frac{\partial c}{\partial t} = A \times D_B \frac{\partial c}{\partial x}\Big|_{x+\Delta x} - A \times D_B \frac{\partial c}{\partial x}\Big|_{x} - \Delta V \frac{\mu_m c}{K_c + c} \frac{X}{Y} \tag{2.11}$$

$\dot{M}$ = change in mass of substrate with time (g/d)

ΔV = incremental biofilm control volume (m^3) = A × Δx

t = time ($days^{-1}$)

A = biofilm area planar to x (m^2)

Δx = incremental distance into biofilm (m)

By assuming the planar area (A) is constant, dividing all terms by the incremental control volume ($\Delta V = A \times \Delta x$) and taking the limit as Δx approaches zero results in the partial differential Equation 2.12. Solving this partial differential equation requires two boundary conditions that will vary from system to system (Grady et al., 2011).

$$\frac{\partial c}{\partial t} = D_B \frac{\partial^2 c}{\partial x^2} - \frac{\mu_m c}{K_c + c} \frac{X}{Y} \tag{2.12}$$

Equation 2.12 is a second order non-linear partial differential equation that is difficult to solve. Many modelers use a steady-state assumption by assuming that the change in substrate concentration with respect to time ($\partial c/\partial t$) is zero. This assumption is made in order to simplify the underlining mathematics required for solving the model; however, this assumption only applies to systems where the substrate bulk liquid concentration remains constant. Other simplification techniques include modeling the kinetics as first-order instead of Monod kinetics, pseudoanalytical approaches, and the effectiveness factor approach, to name a few (Grady et al., 2011). A majority of these simplifications are geared towards simplifying the mathematics required to solve the model.

CHAPTER 3. MOORHEAD WWTF AND PREVIOUS STUDY EFFORTS

Background on the Moorhead WWTF and the nitrifying MBBR system is provided in this chapter. Additionally, previous study efforts focused on better understanding of the Moorhead MBBR are discussed within this chapter. This study builds from the previous study efforts and utilizes data collected during the previous efforts.

3.1. Moorhead WWTF and Nitrifying MBBR

Since 1983, the City of Moorhead, Minnesota has operated a WWTF with a design capacity of 22,710 m^3/d, with the latest rounds of upgrades completed in 2009. The Moorhead WWTF has liquid treatment processes with continuous discharges into the Red River of the North (Red River) and solids treatment processes with ultimate land application as biosolids (City of Moorhead, MN, 2012). A flow diagram for the facility is shown in Figure 3.1.

At the Moorhead WWTF, the liquid treatment processes include primary treatment with bar screens, aerated grit tanks, flow equalization, and primary clarification. Secondary treatment is achieved with a high purity oxygen activated sludge system and final clarification. Post-secondary treatment is accomplished with a MBBR for nitrification, polishing ponds, and combined chlorination-dechlorination for seasonal disinfection prior to discharge into the Red River. The solids treatment processes include sludge thickening, anaerobic digestions with gas recovery to convert the sludge into biosolids. The solids treatment then involves biosolids storage and dewatering with the biosolids ultimately being land applied. Annually, 400 to 800 acres of farmland receive biosolids from the Moorhead WWTF (City of Moorhead, MN, 2012).

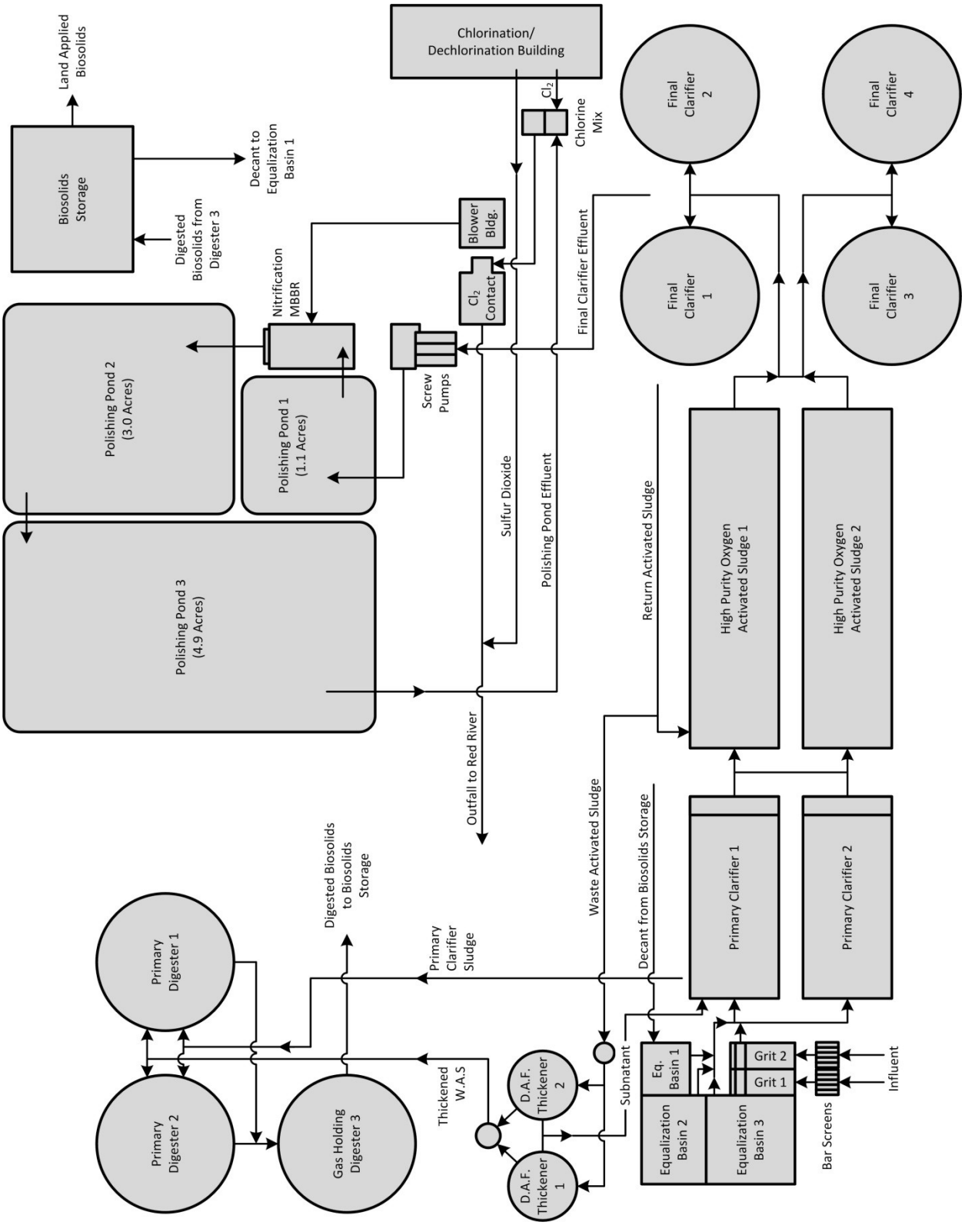

Figure 3.1. Moorhead WWTF flow diagram (Source: Zimmerman et al., 2005)

The nitrifying MBBR was constructed in 2003 due to new seasonal ammonia-N limits being incorporated into the National Pollutant Discharge Elimination System (NDPDES) permit for the facility. The seasonal NDPDES limits (Table 3.1) are flow rate based and result in a significantly reduced mass limit at low river flow rates (Zimmerman et al., 2005).

Table 3.1. Moorhead WWTF effluent ammonia-N limits (Source: Zimmerman et al., 2005)

Effective Period	Applicable River Flow Rate	Limit Type	Limit
June through September	All River Flow Rates	Calendar Month Average	19 mg/L
	Greater than 1.42 m^3/s	Calendar Month Average	647 kg/d
	Less than 1.42 m^3/s	Calendar Month Average	108 kg/d

The Moorhead MBBR was the first post-secondary treatment MBBR installation in the United States (City of Moorhead, MN, 2012). Because of the novelty of the post-secondary MBBR installation, a pilot study was conducted to verify process feasibility and confirm important design criteria. Overall, the MBBR process was selected as the preferred alternative for treating ammonia because it did not alter the plant capacity, the process fit well with the existing plant facilities, and could easily be expanded to meet future demands (with the addition of extra media) (Zimmerman et al., 2005). The design criteria for the Moorhead MBBR system are presented in Table 3.2.

The size of the Moorhead MBBR basin is 42 m by 24.4 m with a design water depth of 2.9 m, resulting in a total volume of 2,970 m^3. The Moorhead MBBR was designed for a current peak month flow rate of 24,610 m^3/d and a future peak month flow rate of 34,075 m^3/d with the installation of additional media. The system was designed for an influent ammonia-N concentration of 17 mg/L, a current peak month ammonia-N loading rate of 417 kg/d, and a future peak month loading rate of 578 kg/d. The predicted ammonia-N removal rate was

between approximately 65 and 81 percent, resulting in an effluent ammonia-N concentration between 3.2 and 6.0 mg/L. A diagram of the Moorhead MBBR system is shown in Figure 3.2.

Table 3.2. Moorhead MBBR design criteria (Source: Zimmerman et al., 2005)

	Initial		Future	
Parameter	**Average**	**Peak Month**	**Average**	**Peak Month**
Basin Dimensions (m)	42 × 24.4 × 2.9 (length × width × depth)			
Basin Volume (m^3)	2,970			
Media Size (mm)	21 × 15 (diameter × length)			
Total Media Volume (m^3)	938	938	938	1,614
Media Volume (Percent Fill)	32	32	32	54
Flow Rate (m^3/d)	18,173	24,610	22,710	34,075
Influent Ammonia-N Concentration (mg/L)	17	17	17	17
Influent Ammonia-N Loading Rate (kg/d)	308	417	385	578
Influent Ammonia-N Loading Rate (g/m^2-d)	0.84	1.13	1.04	0.91
Predicted Average Removal Rate (g/m^2-d)	0.70	0.85	0.81	0.74
Effluent Ammonia-N Concentration (mg/L)	6.0	4.4	4.8	3.2
Effluent Ammonia-N Loading Rate (kg/d)	108	108	108	108
Oxygen Required (kg/d)	1,185	1,428	1,363	2,156
Air for Oxygen (std. m^3/min)	125	151	144	228

The MBBR is currently 32 percent filled with media and designed to ultimately be filled up to 54 percent. The media has a specific surface area of 568 m^2/m^3 and an internally protected surface area of 388 m^2/m^3. In the wake of recent flooding, some of the media was lost and has been replaced with new media that is 1.0 mm longer that the existing media; however, at the time of the biofilm analysis and bench-scale trials discussed during this study, only the original media was presented in the system. The media provides a surface for nitrifying bacteria to grow and a screening system on the discharge now keeps the media in the basin. The aeration system is designed to deliver 228 standard m^3/min of air providing the required oxygen needed for nitrification and to keep the system well mixed. The aeration system is shown in Figure 3.2.

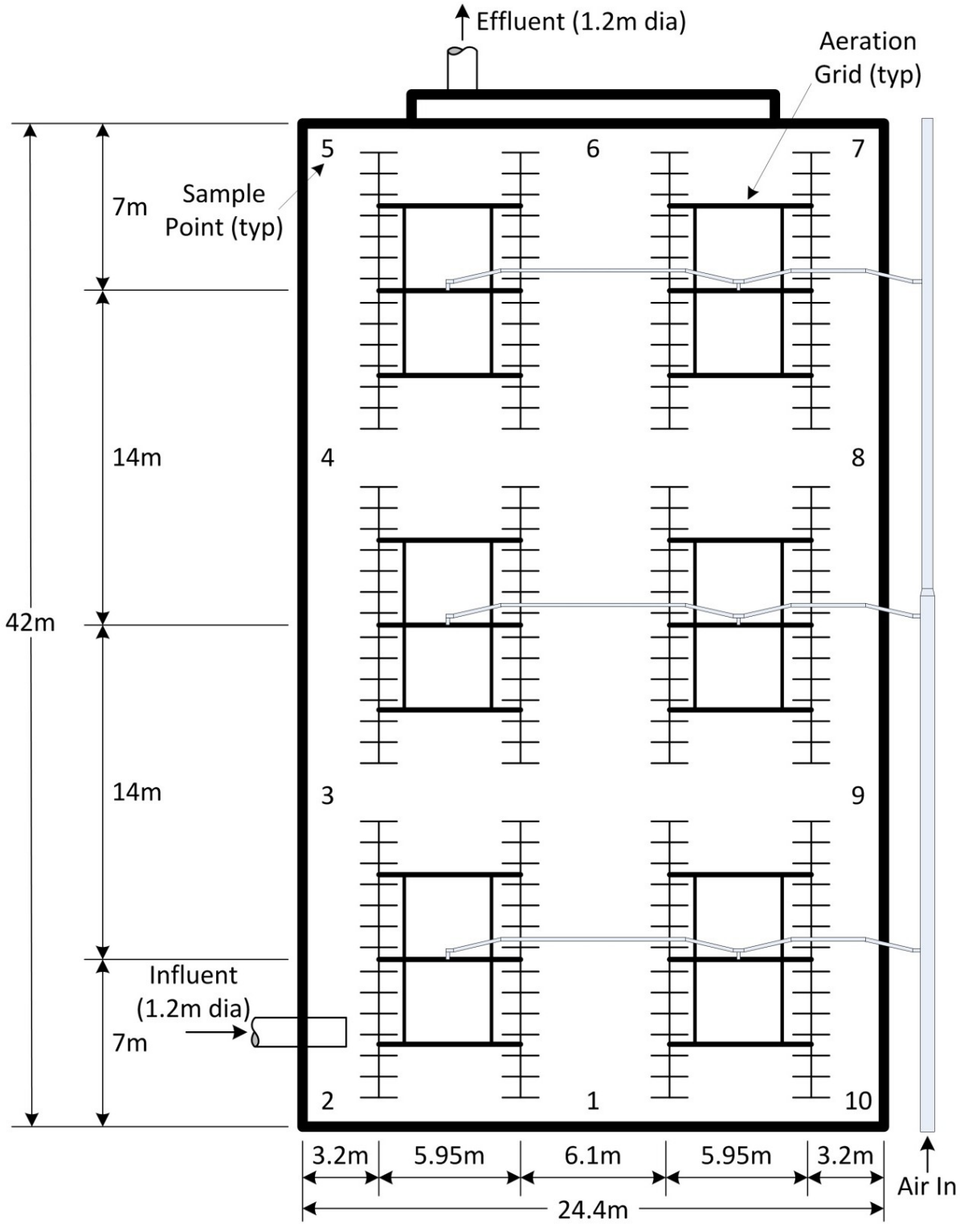

Figure 3.2. Moorhead MBBR schematic (Source: Zimmerman et al., 2005)

Since operation of the Moorhead MBBR has begun, the influent loading has been highly variable and has consistently exceeded the design loading rate. Monthly average influent ammonia-N concentrations in excess of 30 mg/L have been observed, nearly doubling the 17 mg/L design value. However, the system has been able to achieve the designed effluent concentration meeting the permit limits during the June through September enforcement duration. Additionally, performance was only slightly reduced during colder weather months when permit limits are not enforced (Zimmerman et al., 2005). This observation was discussed in Chapter 1.

3.2. Previous Moorhead MBBR Study Efforts

Biofilm characteristics, including biomass per unit medium surface area (biomass per unit area), volatile solids percentage of the biomass, apparent biofilm thickness, and specific biofilm surface length, were monitored and recorded in previous study efforts. These characteristics have been recorded along with the water temperature providing an excellent data source for studying the temperature impacts on the Moorhead MBBR. Additionally, a series of bench-scale trials was performed in an effort to study the nitrification rates in the Moorhead MBBR at various temperatures. The monitored biofilm characteristics and bench-scale trial results form the data set required for this research effort. The following sections discuss the processes that have been done to collect the biofilm characteristics data, for performing the bench-scale trials, and the results of previous nitrification kinetic modeling.

3.2.1. Fixed Film Biomass Monitoring

A procedure for determining the unit biomass attached to the media was obtained from Hydroxyl Systems, Inc.; the manufacturer of the media. The procedure involved taking four active media samples from the Moorhead MBBR and then drying the samples for a minimum of two hours at 104 °C until no additional weight loss was observed. After allowing the samples to cool, the samples are weighed with the dried biomass still attached. Then the media undergo a cleaning process that involves soaking in bleach for two hours and then manually cleaning them with a brush and finally rinsing. The media are then dried for an additional two hours at 104 °C, allowed to cool, and weighed. By knowing that each media has an internally protected area of 0.003492 m^2, the weight difference between before and after the cleaning divided by the product of four times the protected area per media yields the amount of biomass per unit area (g/m^2) (Bjornberg, 2009).

A separate test was added to determine the volatile percent of the attached biomass. The procedure involved collecting the biomass that was scrubbed off during the media cleaning process. The biomass was separated from the liquid using a glass microfiber filter, dried at 104 °C for one hour, allowed to cool for one hour and then weighed. The biomass was then planed in a muffle furnace at 500 °C for one hour. After cooling at 104 °C and in a in a desiccator, the burnt filter was weighed a final time. The change in mass during the process corresponds to the percentage of volatile solids in the attached biomass. In total, 17 volatile solids samples were conducted resulting in a range from 26.3 to 49.4 percent of the total biomass was volatile, with an average of 38.3 percent (Bjornberg, 2009). There is not an apparent trend in the volatile solids sampling, and a volatile solids percentage of 40 percent is assumed for this research effort.

3.2.2. Biofilm Characteristics Monitoring

To determine the apparent biofilm thickness and surface area, a process using image analysis software was employed. Three media samples were taken weekly from the Moorhead MBBR and placed under a dissecting microscope for analysis and photography. The procedure involved taking 17 pictures at various locations and cross sections along the media for each of the three media samples. Examples of such photographs are shown in Figure 3.3. ImageJ, an image analysis software developed by the National Institute of Health, was used to record three distinct measurements for each photo: (1) the cross-sectional area of the biofilm (A_i), (2) the biofilm surface length (P_b), and (3) the media sample length (P_m). The measured values were averaged between the three weekly media samples. A schematic of these three measurements is shown in Figure 3.4 (Bjornberg, 2009).

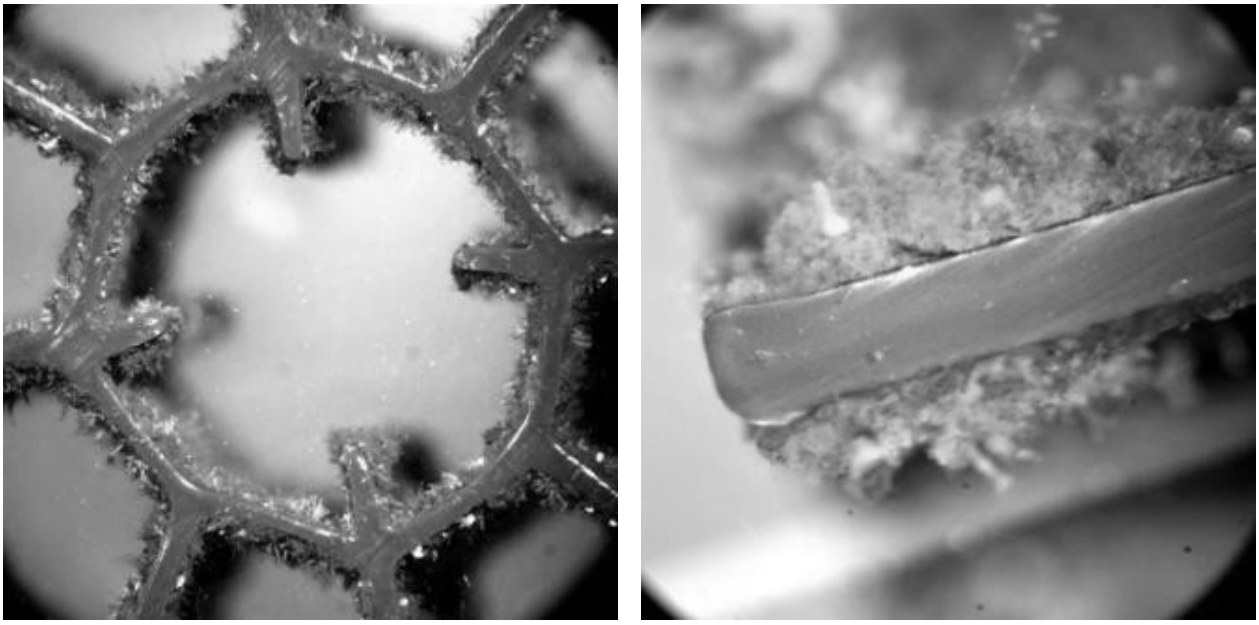

Figure 3.3. Example image analysis of biofilm (Source: Bjornberg, 2009)

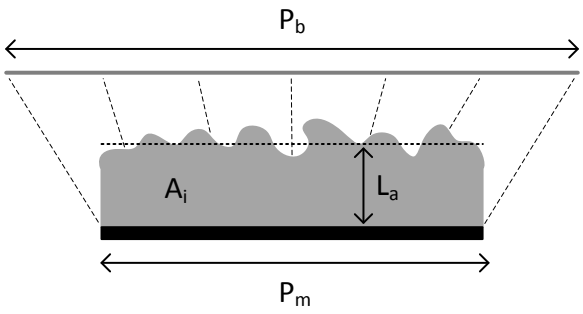

Figure 3.4. Biofilm image analysis diagram

The apparent biofilm thickness (L_a) is determined from the image analysis by dividing the cross-sectional area of the biofilm (A_i) by the media sample length (P_m). This relationship is shown as Equation 3.1. The specific biofilm surface length (S_{SL}) is the ratio of the biofilm surface length (P_b) to the media sample length (P_m) as presented as Equation 3.2.

$$L_a = A_i/P_m \tag{3.1}$$

L_a = apparent biofilm thickness (m)

A_i = biofilm cross-sectional area from image analysis (m^2)

P_m = media sample length from image analysis (m)

$$S_{SL} = P_b/P_m \tag{3.2}$$

S_{SL} = specific biofilm surface length (m/m)

P_b = biofilm surface length from image analysis (m)

3.2.3. Bench-Scale Kinetic Trials

To study the ammonia removal rates at different temperatures, a series of bench-scale trials were performed. Each trial involved pulling active media directly from the full-scale Moorhead MBBR right before the experiment and running the reactor as a batch system with matching media fill, temperature, and airflow rates to mimic operating conditions of the MBBR. A diagram of the reactor setup for the nitrification bench-scale trials is shown in Figure 3.5.

Prior to running each test, a non-nitrified water sample was taken from Polishing Pond 1 effluent. Active media was then filled to the 1.8 L mark on the reactor and the remaining reactor was filled up to the 6.0 L mark with the non-nitrified sample. This equated to approximately a 32 percent media fill, matching the full-scale MBBR. The temperature was maintained by running the reactor in an incubator and consistent airflow rates maintained using an airflow meter. Ammonia-N was then measured at 15-minute time intervals until the concentration was less than 0.5 mg/L. In addition to the biofilm characteristics previously described, sampling during the trials included dissolved oxygen, suspended solids, volatile suspended solids, pH, alkalinity, nitrite-N, and nitrate-N. Bench-scale trials were duplicated to help ensure consistent results, with a total of 12 trials performed at varying water temperatures between 10 °C and 20 °C. A summary of the bench-scale trials and associated biofilm characteristics is shown in Table 3.3 (Bjornberg, 2009).

Monitoring of the full-scale system was also performed as part of the previous study efforts. The same biofilm characteristics were measured weekly from media taken from the full-scale MBBR (Bjornberg, 2009). Additional daily and weekly sampling data and flow rates are also available from the Moorhead MBBR during this timeframe.

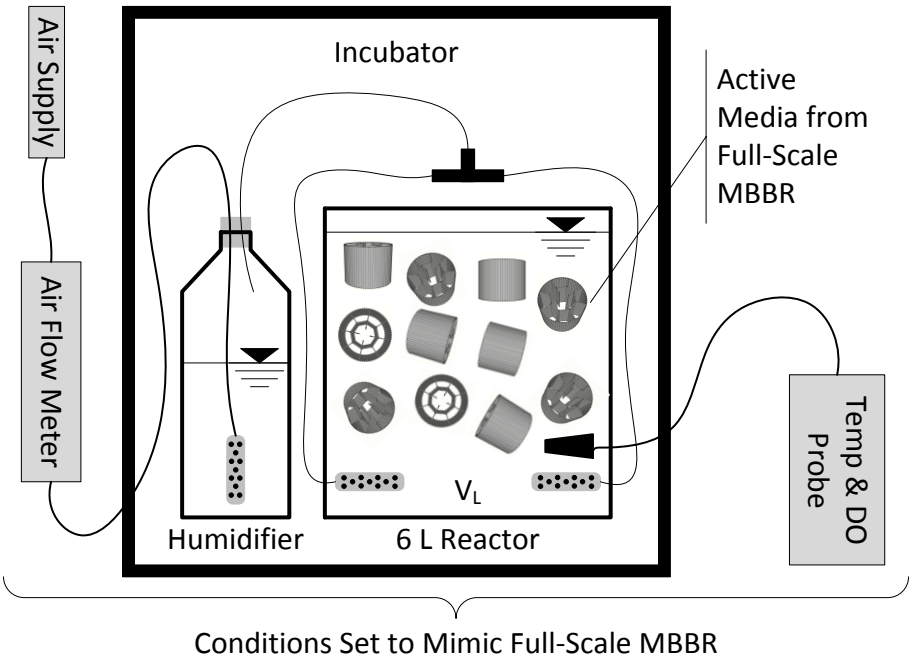

Figure 3.5. Nitrification bench-scale trials reactor diagram (Source: Bjornberg, 2009)

Table 3.3. Bench-scale trials and biofilm characteristics summary

Trial Information			Attached Biomass and Biofilm Characteristics		
#	Water Temperature (°C)	Duration (min)	Unit Biomass (g/m^2)	Average Thickness (µm)	Specific Surface Length (m/m)
1	20	330	7.51	62.90	2.20
2	20	330	7.39		
3	19	225	7.46	68.70	2.10
4	19	210	7.40		
5	15	195	6.88	53.10	2.40
6	16	180	7.26		
7	14	225	9.66	103.20	2.80
8	15	225	9.83		
9	11	180	14.35	153.70	3.40
10	11	180	14.11		
11	10	300	18.67	216.30	3.70
12	10	255	18.87		

3.2.4. Summary of Previous Study Efforts

Previous study efforts on the Moorhead MBBR observed seasonal changes in the biofilm thickness and biofilm surface area and affirmed that changes in the season and temperature result in significant changes in the amount of attached biomass. Based on the information in Table 3.3, previous efforts observed that as the temperature decreased the amount of attached biomass, the biofilm thickness, and the biofilm surface area all increased. Additionally, a series of kinetic trials was performed in an effort to determine the impact of temperature on nitrification kinetics. The collected data from the previous study efforts that has been used for this study is included in Appendix A. A model was developed using the kinetic trial data and provided a good initial effort at modeling MBBR fixed film nitrification kinetics; however, some questions remained to be answered (Bjornberg et al., 2010). As such, this research effort was undertaken to ultimately develop better kinetic models that incorporated the observed changes in attached biomass, changes biofilm thickness, and changes in biofilm surface area previously discussed.

CHAPTER 4. METHODOLOGY AND MODEL DEVELOPMENT

The approach for addressing the three goals of this study is contained in this chapter and includes discussions focused on analysis of biofilm characteristics, mathematical model development, and the approach to solve the model using the bench-scale trial results. Additional discussions as part of the model solution procedure include how to evaluate the temperature impacts to Monod kinetics for fixed film applications.

4.1. Biofilm Characteristics Analysis

In order to address the first goal of this study, the biofilm characteristics that were measured and recorded in prior research efforts (Section 3.2) are analyzed for potential relationships between the specific parameters and for temperature impacts on these parameters. These parameters include biomass per unit area, apparent biofilm thickness, specific biofilm surface length, specific biofilm surface area, and biomass density. The analyses involve implementing least squares techniques to determine the relationships between temperature and the biofilm characteristics, and to determine the relationships between the different biofilm parameters. This approach will involve testing potential relationships against the observed data and determining the best-fit potential relationship by minimizing the sum of the squared residuals (sum of the squared differences between the observed values and predicted values). The coefficients of determination (R^2) will be used to evaluate the goodness of fits between the relationships and the observed data. Coefficients of determination indicate how well the predicted data fits the observed data, with a value of 1.0 indicating a perfect fit. The measured biofilm parameters and the results of the analyses will be included as part of the model development and used as input for the model simulations. It should be noted that the biomass

density was not measured and needs to be calculated using other measured parameters. The equation for calculated density is included as part of the model development section, and is presented as Equation 4.38 for the total solids and as Equation 4.40 for the volatile solids.

4.2. Unsteady-State Biofilm Model Development

To meet the second and third goals of this study, a mathematical model that incorporates both diffusion and reaction in the biofilm needs to be developed to simulate nitrification in the bench-scale trials. The model must also be able to incorporate the biofilm characteristics and provide insight into how temperature affects the kinetic parameters. Accomplishing these tasks requires the development of two models that must be solved simultaneously: (1) a system model to simulate the bulk ammonia-N concentration change with time in the bench-scale reactor, and (2) a biofilm model to simulate the attached biomass, the ammonia-N diffusion through the biofilm, and the ammonia-N utilization. The following sections describe the geometric biofilm approximation method, development of the system model, development of the biofilm model, and a summary of the overall unsteady-state model.

4.2.1. Biofilm Geometric Approximation

In order to develop the model, the geometry of the biofilm needs to be simplified. From the image analysis, the volume of the biofilm (V_B) can be calculated by multiplying the biofilm average thickness (L_a) by the protected media surface area in the reactor (A_m). This relationship is shown as Equation 4.1. Because the same percent media fill is used in the all bench-scale trials, the protected media surface area (A_m) is constant and is equal 0.698 m^2. Additionally, the

model does not consider non-protected or external media area and the protected media surface area will be referred to as the media surface area herein.

$$V_B = L_a \times A_m \tag{4.1}$$

V_B = volume of biomass in reactor (m^3)

L_a = apparent biofilm thickness (m)

A_m = media surface area in reactor (m^2)

The biofilm shape is approximated as a square truncated pyramid (base portion of a pyramid) shape by stretch out the biofilm surface as shown in Figure 4.1 and Figure 4.2. The side lengths of the pyramid approximation correspond to the biofilm surface length from image analysis (P_b) and media sample length from image analysis (P_m). Assuming that the curvature is the same in all directions, then the total biofilm surface area (A_b) can be calculate by multiplying the media surface area (A_m) by the square of the specific surface length (S_{SL}) following Equation 4.2. Using this assumption, the specific surface area (S_{SA}) can be derived as the ratio between the total biofilm surface area (A_b) in the reactor and the media surface area (A_m) in the reactor. The specific surface area (S_{SA}) is also equal to the square of the specific surface length (S_{SL}). These relationships are shown in Equation 4.2 and Equation 4.3 and graphically in Figure 4.1 and Figure 4.2.

$$A_b = A_m \times {S_{SL}}^2 = A_m \times S_{SA} \tag{4.2}$$

A_b = biofilm surface area in reactor based on pyramid approximation (m^2)

A_m = media surface area in reactor (m^2)

S_{SL} = specific surface length (m/m)

S_{SA} = specific surface area (m^2/m^2)

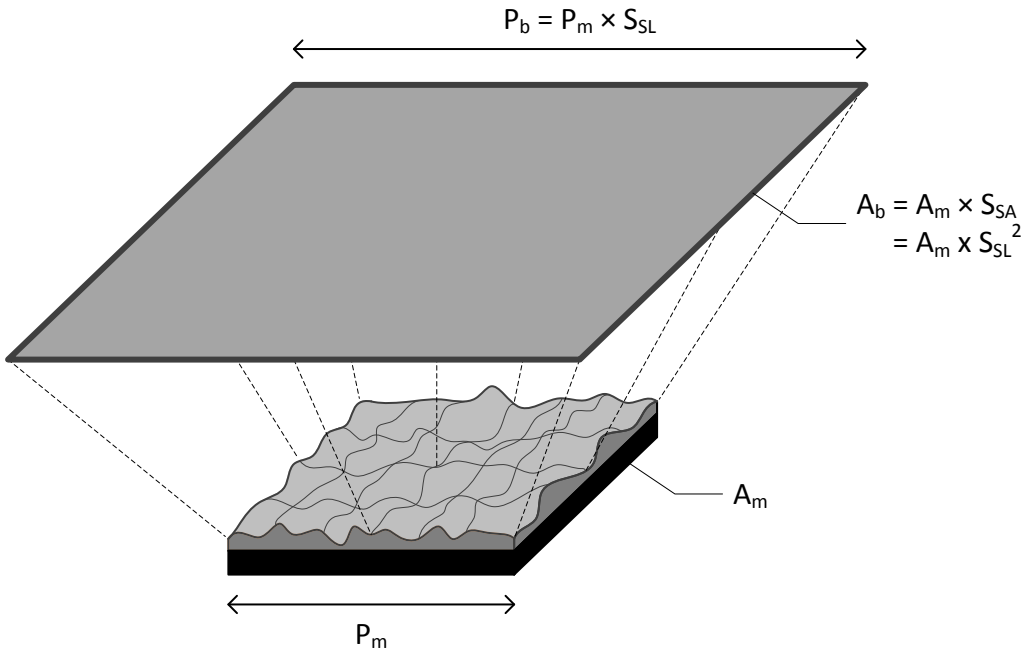

Figure 4.1. Diagram of biofilm square truncated pyramid approximation

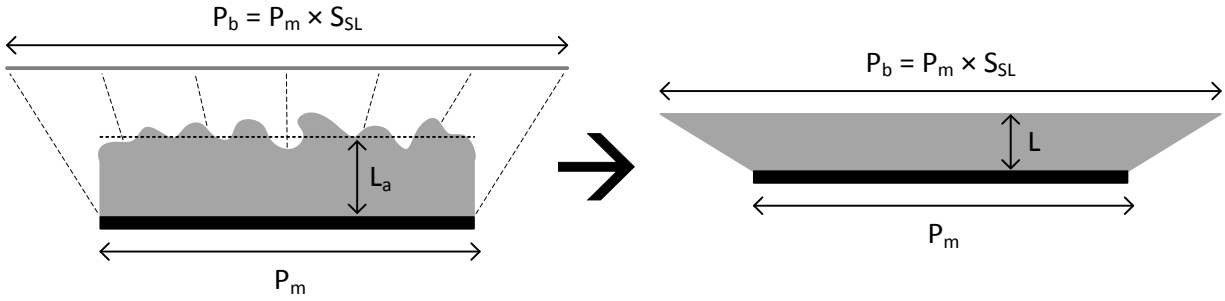

Figure 4.2. Diagram of the biofilm square truncated pyramid approximation profile

$$S_{SA} = \left(\frac{P_b}{P_m}\right)^2 = \frac{A_b}{A_m} = {S_{SL}}^2 \tag{4.3}$$

P_b = biofilm surface length from image analysis (m)

P_m = media sample length from image analysis (m)

The volume of a square truncated pyramid (V_{pyr}) is given by Equation 4.4 and is a function of the pyramid height (h), and the side length of top (b) and bottom (a) surfaces. A representative diagram of a square truncated pyramid is shown in Figure 4.3.

$$V_{pyr} = \frac{1}{3}(a^2 + ab + b^2) \times h \tag{4.4}$$

V_{pyr} = volume of truncated pyramid

a = side length of bottom surface

b = side length of top surface

h = pyramid height

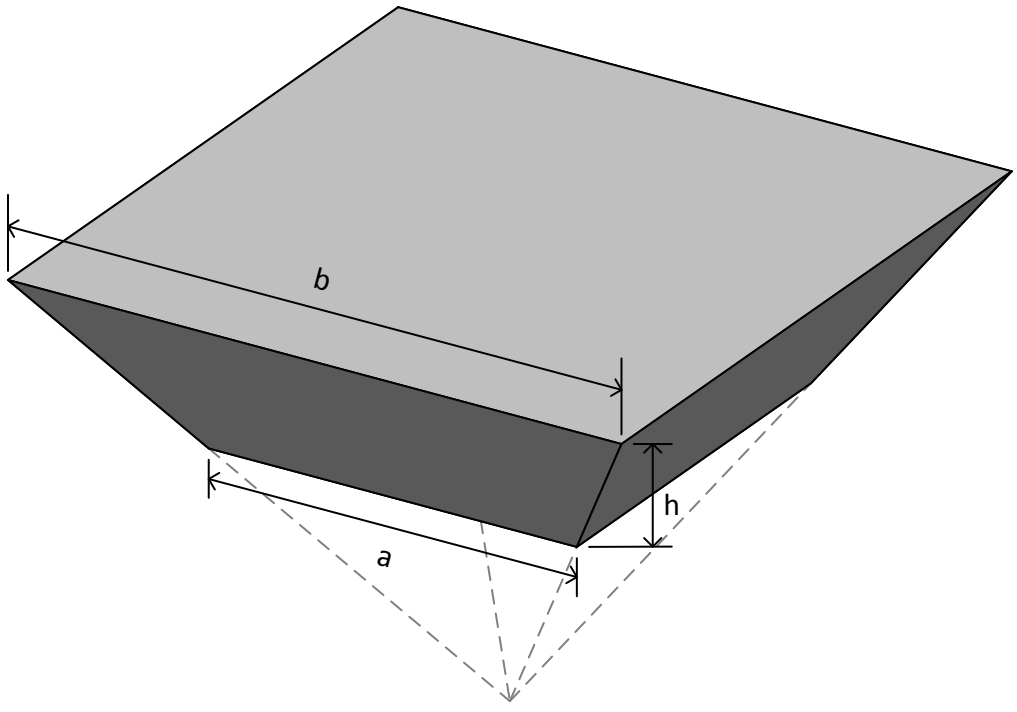

Figure 4.3. Square truncated pyramid diagram

Using Equation 4.4, the volume of the biofilm (V_b) can be calculated, where the bottom and top lengths are P_m and P_b, respectively, and the height is the biofilm thickness based on the pyramid approximation (L), which will be referred to as the biofilm thickness herein. The volume of the biofilm calculated from the truncated pyramid approximation must equal the biofilm volume determined from the image analysis. This relationship is shown as Equation 4.5. Solving the equation for the biofilm thickness (L) results in Equation 4.6. P_m^2 can then be factored out the denominator resulting in Equation 4.7. It should be noted, that the apparent biofilm thickness (L_a) from the image analysis is not equal to the biofilm thickness (L). Because the pyramid approximation is used to simplify the biofilm geometry in the model, the biofilm thickness (L) is used as the thickness of the biofilm in the unsteady-state model.

$$V_b = \frac{1}{3}\left({P_m}^2 + P_m P_b + {P_b}^2\right) \times L = A_m \times L_a \tag{4.5}$$

L = biofilm thickness [based in the truncated pyramid approximation] (m)

$$L = \frac{3 \times A_m \times L_a}{{P_m}^2 + P_m \times P_b + {P_b}^2} \tag{4.6}$$

$$L = \frac{3 \times A_m \times L_a}{{P_m}^2 \left(1 + \frac{P_b}{P_m} + \left(\frac{P_b}{P_m}\right)^2\right)} \tag{4.7}$$

Recognizing that the media surface area (A_m) is equal to the square of the media sample length (P_m) from the relationship presented in Equation 4.3, A_m can be substituted into Equation 4.7 resulting in Equation 4.8. Simplification yields Equation 4.9 for the biofilm thickness (L).

$$L = \frac{3 \times {P_m}^2 \times L_a}{{P_m}^2\left(1 + S_{SL} + {S_{SL}}^2\right)} \tag{4.8}$$

$$L = \frac{3 \times L_a}{\left(1 + S_{SL} + {S_{SL}}^2\right)} \tag{4.9}$$

The liquid volume in the reactor can be calculated by subtracting the media volume (V_m), which is known from the bench-trials, and the biomass volume (V_B) from the total volume of the reactor (V_T). This relationship is shown as Equation 4.10. The total reactor volume (V_T) for all bench-scale trials was 6.0 L and because the percent media fill was the same between the trials, the media volume (V_m) in the reactor for all trials was 0.192 L. The biofilm volume (V_B) is calculated for each trial following Equation 4.1.

$$V_L = V_T - V_B - V_m \tag{4.10}$$

V_L = liquid volume in reactor (m^3)

V_T = total volume of reactor (m^3)

V_m = media volume in reactor (m^3)

4.2.2. System Model Development

The system model for the bench-scale trials was developed by assuming a completely mixed batch system and assuming the system is single substrate limited (assumes sufficient oxygen and alkalinity are present and non-inhibitory for nitrification). Performing a mass-balance around the bulk liquid volume in the reactor (V_L) indicates that the change in ammonia-N mass in the bulk liquid is equal to the ammonia-N flux (J_N) out of the bulk liquid multiplied by

the biofilm surface area (A_b). The mass-balance is shown as Equation 4.11 and a diagram of the system model is presented as Figure 4.4.

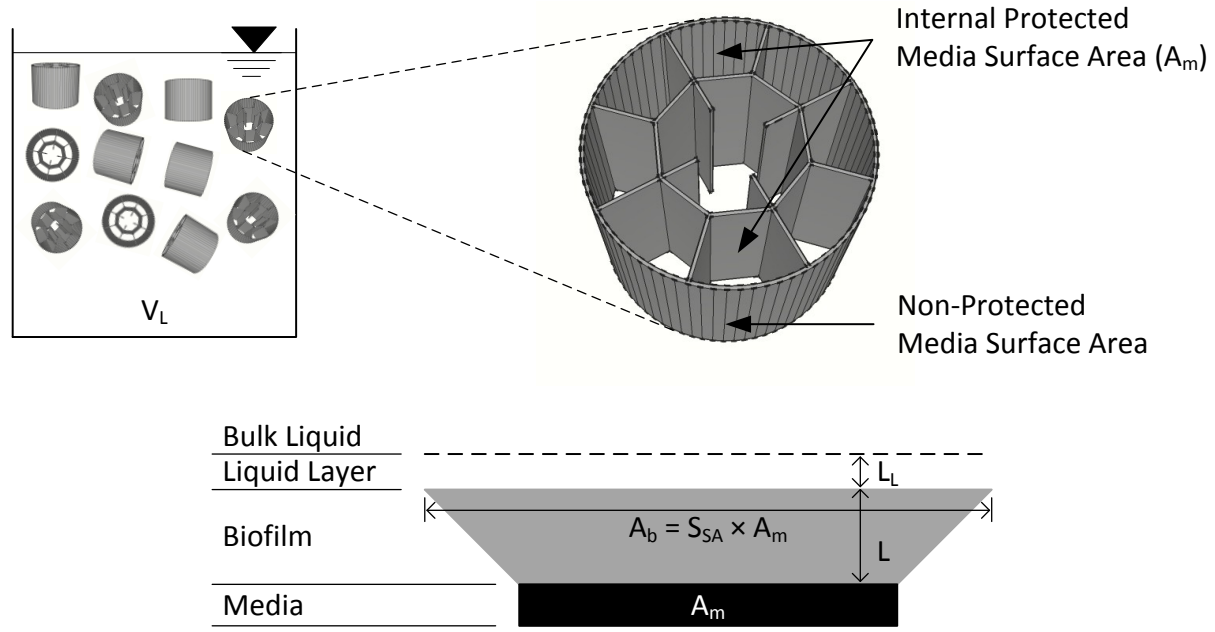

Figure 4.4. System model diagram

$$\dot{M} = V_L \frac{dN}{dt} = -J_N \times A_b \tag{4.11}$$

$\dot{M}$ = change in mass of ammonia-N with time (g/d)

N = ammonia-N concentration (g/m^3)

t = time (d)

J_N = unit ammonia-N flux (g/m^2-d)

The ammonia-N flux (J_N) out of the bulk liquid is modeled by implementing a hypothetical stagnant liquid layer immediately outside of the biofilm with ammonia-N

concentration N_b equating to the bulk concentration and N_s corresponding to the concentration at the surface of the biofilm. At the interface between the stagnant liquid layer and the biofilm, the ammonia-N flux (J_N) across the stagnant liquid layer is equal to the flux into the biofilm. The ammonia-N flux across the stagnant liquid layer is approximated by difference in concentration on either side of the stagnant liquid layer multiplied by the substrate diffusion coefficient in water (D_W) divide by the thickness of the stagnant liquid layer (L_L). This relationship is presented mathematically as Equation 2.9 and shown again as Equation 4.12 specific to ammonia-N as the substrate.

$$J_c = \frac{D_W}{L_L}(N_b - N_s) \tag{4.12}$$

D_W = substrate diffusion coefficient in water (m^2/d)

L_L = thickness of stagnant liquid layer (m)

N_b = bulk liquid ammonia-N concentration (g/m^3)

N_s = ammonia-N concentration at liquid-biofilm interface (g/m^3)

Combining Equations 4.2, 4.11, and 4.12 results in the system model presented as Equation 4.13. The sign convention of the system model is used to indicate the direction of mass transport out of the bulk liquid and into the biofilm.

$$V_L \frac{dN}{dt} = -\frac{D_W}{L_L}(N_b - N_s) \times A_m \times {S_{SL}}^2 \tag{4.13}$$

The ammonia-N diffusion coefficient in water (D_W) is linearly related to temperature and ranges from 1.10×10^{-4} m^2/d at 10 °C to 1.49×10^{-4} m^2/d at 20 °C (Stewert, 2003). The linear

equation developed utilizing these values is shown as Equation 4.14 where the diffusion coefficient (D_W) in water is a function of temperature (T). This equation is used for this modeling effort.

$$D_W = 3.87 \times 10^{-6} \times T + 7.10 \times 10^{-5} \quad (4.14)$$

T = water temperature (°C)

The thickness of the stagnant liquid layer (L_L) is hypothetical and cannot be measured directly. As discussed in Section 2.4, a thicker stagnant liquid layer thickness corresponds to an increase in mass transfer resistance out of the bulk liquid. Based on studying the modeling implications of varying the liquid layer thickness, a thickness of 40 μm is assumed. This value is appropriate for a completely mixed system under turbulent flow conditions.

4.2.3. Biofilm Model Development

The model of the biofilm needs to incorporate two components: (1) a diffusion component accounting for mass transfer into and through the biofilm, and (2) a biological degradation model to account for ammonia-N utilization and uptake. Both components are needed to properly model the ammonia-N removal from the bench-scale trials. To account for these phenomena a model that combines diffusion and Monod kinetics are commonly used (Grady et al., 2011). In the model, the ammonia-N concentration N is a function of both time (t) and position (x). A diagram of the biofilm model development is shown in Figure 4.5.

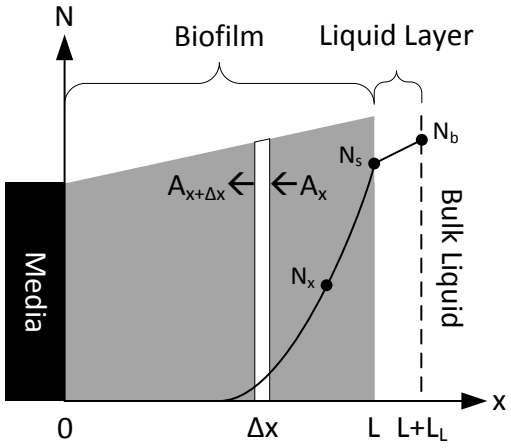

Figure 4.5. Biofilm model diagram

The basis for the biofilm model involves performing a substrate mass-balance around a control volume within the biofilm. The change in ammonia-N mass ($\dot{M}$) within the control volume can be expressed as the control volume ($\Delta V = A \times \Delta x$) multiplied by the change in ammonia-N concentration with time (dN/dt). This equals to the ammonia-N flux (J_N) into the control volume multiplied by the diffusional area (A) at location x minus the ammonia-N flux (J_N) out of the biofilm multiplied by the diffusional area (A) at location x+Δx less any ammonia-N removal due to biological degradation within the control volume. For simplicity, the biological degradation is represented as a function (r) multiplied by the control volume (ΔV). Because of the truncated pyramid approximation for the biofilm, the diffusion area is not constant and is a function of the distance into the biofilm and is represented as the function A(x). The mathematical representation of the control volume mass-balance is shown as Equation 4.15.

$$\dot{M} = \Delta V \frac{dN}{dt} = A(x) \times J_N|_x - A(x + \Delta x) \times J_N|_{x+\Delta x} - r \times \Delta V \tag{4.15}$$

ΔV = incremental biofilm control volume (m^3)

A(x) = biofilm diffusional area as a function of x (m^2)

x = distance into biofilm (m)

Δx = incremental distance into biofilm (m)

r = ammonia-N remove function (g/d)

Fick's first law of diffusion, previously shown as Equation 2.10 and shown again as Equation 4.16, is used to model the ammonia-N flux (J_N) in the biofilm model. Fick's first law relates the ammonia-N flux (J_N) to an effective substrate diffusion coefficient (D_B) multiplied by the concentration gradient (dN/dx) within the biofilm.

$$J_c = -D_B \frac{dN}{dx} \tag{4.16}$$

D_B = effective ammonia-N diffusion coefficient in the biofilm (m^2/d)

The substitution of Fick's first law of diffusion (Equation 4.16) into the biofilm control volume mass-balance equation results in Equation 4.17 where the flux terms has been replaced with the effective diffusion coefficient (D_B) multiplied by the concentration gradient (∂N/∂x) at locations x and x+Δx.

$$\dot{M} = \Delta V \frac{\partial N}{\partial t} = A(x + \Delta x) \times D_B \frac{\partial N}{\partial x}\Big|_{x+\Delta x} - A(x) \times D_B \frac{\partial N}{\partial x}\Big|_{x} - \Delta V \times r \tag{4.17}$$

Based on the truncated pyramid biofilm approximation, an equation for the biofilm diffusional area (A) as a function of position (x) can be developed. The slope of the linear

equation for A(x) is equal to the difference between the biofilm surface area (A_b) and the media surface area (A_m) divided by the apparent biofilm thickness (L). The intercept of the line is simply the media surface area (A_m), resulting in Equation 4.18 representing the function A(x). The equation for the diffusional area can be further simplified by replacing the biofilm surface area (A_b) with Equation 4.2 to incorporate the specific surface area (S_{SA}).

$$A(x) = \frac{A_b - A_m}{L} x + A_m \tag{4.18}$$

$$A(x) = \frac{A_m \times (S_{SA} - 1)}{L} x + A_m \tag{4.19}$$

The control volume (ΔV) is calculated by multiplying the thickness of the control volume, previously defined as the incremental distance (Δx) into the biofilm, by the planar area at the midpoint of the control volume (x+Δx/2), which calculated using the function A(x). The equation for the control volume (ΔV) is presented as Equation 4.20. Equation 4.20 can then be substituted into the control volume mass-balance equation resulting in Equation 4.21. Further simplification by factoring out the constant effective diffusion coefficient (D_B) and dividing by the incremental distance (Δx) results in Equation 4.22.

$$\Delta V = A(x + \Delta x/2) \times \Delta x \tag{4.20}$$

$$A(x + \Delta x/2) \times \Delta x \frac{\partial N}{\partial t} = A(x + \Delta x) \times D_B \frac{\partial N}{\partial x}\Big|_{x+\Delta x} - A(x) \times D_B \frac{\partial N}{\partial x}\Big|_{x} - A(x + \Delta x/2) \times \Delta x \times r \tag{4.21}$$

$$A(x + \Delta x/2) \frac{\partial N}{\partial t} = D_B \left(A(x + \Delta x) \frac{\partial N}{\partial x}\Big|_{x+\Delta x} - A(x) \frac{\partial N}{\partial x}\Big|_{x} \right) / \Delta x - A(x + \Delta x/2) \times r \tag{4.22}$$

By taking the limit as Δx approaches zero, as shown in Equation 4.23, the control volume mass-balance equation becomes the partial differential Equation 4.24. This equation relates the change in ammonia-N concentration with respect to time ($\partial N/\partial t$) as a function of a diffusion coefficient multiplied by the derivative of the diffusional area function (A(x)) multiplied by the concentration gradient with respect to position ($\partial N/\partial X$) less any ammonia-N removal due to the biological reaction (r). Recognizing that the derivative of a derivative is a second derivate allows for the equation to be further simplified (Equation 4.25) into a form similar to the commonly used modeling equation presented as Equation 2.12; however, is it more convenient to solve the equation in the form show as Equation 4.24 and this form will be used herein.

$$\lim_{\Delta x \to 0}\left[A(x+\Delta x/2)\frac{\partial N}{\partial t}\right] = \lim_{\Delta x \to 0}\left[D_B\left(A(x+\Delta x)\frac{\partial N}{\partial x}\Big|_{x+\Delta x} - A(x)\frac{\partial N}{\partial x}\Big|_{x}\right)/\Delta x - A(x+\Delta x/2)r\right] \quad (4.23)$$

$$A(x)\frac{\partial N}{\partial t} = D_B\frac{\partial}{\partial x}\left(A(x)\frac{\partial N}{\partial x}\right) - A(x)r \quad (4.24)$$

$$A(x)\frac{\partial N}{\partial t} = D_B\frac{\partial A(x)}{\partial x}\frac{\partial^2 N}{\partial x^2} - A(x)r \quad (4.25)$$

The biological degradation is modeled using Monod kinetics as previously shown in Equations 2.5 and 2.6 and represented as Equations 4.26 and 4.27. The Monod kinetics is a set of coupled equations that mode the change in biomass (dX/dt) as well as the change in substrate concentration, in this case ammonia-N concentration (dN/dt), due to biological uptake and degradation, and is an appropriate model for substrate limited conditions such as the bench-scale trials (Grady et al., 2011). Due to the short length of the bench-scale trials, the biomass decay ($k_d \times X$) component of Monod kinetics has been omitted and biomass growth (dX/dt) is assumed negligible, resulting in Equation 4.28 for the biological reaction (r) in the biofilm model. As

such, the Monod kinetics predicts ammonia-N removal with time (dN/dt) as a function of ammonia-N concentration (N), the biomass density (X), the biomass yield coefficient (Y), the half-saturation concentration (K_N), and a maximum specific growth rate (μ_m). The sign change in Equation 4.28 is because the reaction (r) was already shown as a negative in the biofilm model development. After substation of the Monod kinetics from Equation 4.28 into Equation 4.24, the complete equation representing the biofilm system is presented as Equation 4.29.

$$\frac{dX}{dt} = \frac{\mu_m N}{K_N + N} X - k_d X \tag{4.26}$$

$$\frac{dN}{dt} = -\frac{\mu_m N}{K_N + N} \frac{X}{Y} \tag{4.27}$$

μ_m = maximum specific growth rate (d^{-1})

K_N = ammonia-N half-saturation concentration (g/m^3)

X = biomass density (g/m^3)

k_d = endogenous decay coefficient (g biomass / g biomass / d)

Y = ammonia-N yield coefficient (g biomass / g ammonia-N utilized)

$$r = \frac{dc}{dt} = \frac{\mu_m N}{K_c + N} \frac{X}{Y} \tag{4.28}$$

$$A(x) \frac{\partial N}{\partial t} = D_B \frac{\partial}{\partial x} \left(A(x) \frac{\partial N}{\partial x} \right) - A(x) \frac{\mu_m N}{K_c + N} \frac{X}{Y} \tag{4.29}$$

As previously shown (Equation 2.7), the maximum specific substrate utilization rate (k) is often presented and is the maximum specific growth rate (μ_m) divided by the yield coefficient (Y). This can be advantageous because both the maximums specific growth rate (μ_m) and the

yield coefficient (Y) can be solved simultaneously. For ammonia-N utilization, the corresponding equation for the maximum specific ammonia utilization rate (k) is shown in the following equation. This approach will be used in this modeling effort, and then a ammonia-N yield coefficient of 0.25 g-VS/g-N will be utilized to determine the maximum specific growth rates for each bench-scale trial.

$$k = \frac{\mu_m}{Y} \tag{4.30}$$

k = maximum specific ammonia-N utilization rate (g-N/g-VS/d)

In order to solve the biofilm model, two boundary conditions are required. The first boundary condition occurs at the interface between the biofilm and the media (x = 0). Because the substrate cannot penetrate the media, the ammonia-N flux (J_N) at this location equals zero as shown in Equation 4.31. Substituting Fick's first law of diffusion (Equation 4.16) results in the first boundary condition presented as Equation 4.32.

$$J_N|_{x=0} = 0 \tag{4.31}$$

$$-D_B \frac{dN}{dx}\Big|_{x=0} = 0 \tag{4.32}$$

The second boundary condition is more complicated and is based on equating the flux across the stagnant liquid layer to the immediate flux into the biofilm. This flux continuity boundary occurs at the interface between the biofilm and the liquid later (x = L) as shown in Equation 4.33. Substituting the appropriate flux equations for the liquid layer and the biofilm,

with sign convention correlating to mass transport out of the liquid layer and into the biofilm, results in Equation 4.34. This boundary condition also serves to link the biofilm model to the system model.

$$J_N|_{x\to L^-} = J_N|_{x\to L^+} \tag{4.33}$$

$$-D_B \left.\frac{dN}{dx}\right|_{x=L} = \frac{D_W}{L_L}(N_b - N_s) \tag{4.34}$$

As discussed in Section 2.4, to account for the increased mass transport resistance of the biofilm a substrate effective diffusion coefficient that less than the substrate diffusion coefficient in water is often chosen. For this modeling effort, it has been assumed that the effective ammonia-N diffusion coefficient in the biofilm is equal to 60 percent of the ammonia-N diffusion coefficient in water following Equation 4.35.

$$D_B = 0.6D_W \tag{4.35}$$

As part of the biofilm model, the biomass density (X) needs to be determined. The total amount of biomass (M) in the reactor can be determined by multiplying the unit biomass (B) by the media surface area in the reactor (A_m), as shown in Equation 4.36. The biomass density can then be calculated by dividing the total biomass (M) by the biofilm volume (V_B) (Equation 4.37). Combining Equations 4.1, 4.36, and 4.37 results in Equation 4.38 and calculates the total biomass density (X_T) as a function of unit biomass (B) and the apparent biofilm thickness (L_a).

$$M = B \times A_m \tag{4.36}$$

M = biomass in reactor (g)

B = unit biomass (g/m^2)

$$X_T = M/V_B \tag{4.37}$$

X_T = total biomass density (g/m^3)

$$X_T = \frac{B \times A_m}{A_m \times L_a} = \frac{B}{L_a} \tag{4.38}$$

The total biomass density (X_T) calculated in this manner represents the dry biomass divided by the volume of the wet biofilm, and is commonly used in biofilm modeling because of its simplicity to determine. Because the total biomass density includes some inert solids that do not contribute to the substrate degradation, only the volatile portions of the biomass will be considered. To determine the volatile biomass density (X), the total biomass density (X_T) is multiplied by the volatile solids percentage of the biomass (VS), as shown in Equation 4.39. Combined Equations 4.38 and 4.39 results in the complete equation for determined the volatile biomass density (X), presented as Equation 4.40. The volatile biomass density (X) will be used in the model. As previously mentioned, the VS is assumed to be 40 percent, meaning the organic material makes-up 40 percent of the total biomass. Because of the low suspended solids compared to the attached biomass in the reactor, it has also been assumed that only the attached biomass contributes to ammonia-N removal.

$$X = X_T \times VS \tag{4.39}$$

X = [volatile] biomass density (g-VS/m^3)

VS = volatile solids percentage of biomass (%)

$$X = \frac{B \times VS}{L_a} \tag{4.40}$$

4.2.4. Model Development Summary

The biofilm model needs to be solved simultaneously with the system model while adhering to the two boundary conditions in order to determine the solutions to the model. Specifically, the solutions to this coupled model will yield ammonia-N concentrations for different locations within the biofilm as well as the bulk concentration as a function of time for the varying conditions of the bench-scale trials. The equations developed for both the system and biofilm models are summarized in Table 4.1.

4.3. Unsteady-State Model Solution Procedure

Because of the time dependence of the bench-trials, an assumption that the reactor operates in steady state cannot be made. Therefore, numerical analysis must be used to determine the approximate solutions to the models. The numerical analysis technique chosen to solve this model is the Crank-Nicolson Method, which is a finite difference numerical method. For diffusion equations, such as the biofilm model, the Crank-Nicolson Method is unconditionally stable (Press et al., 1986). However, the Crank-Nicolson Method can be more computationally intensive and harder to discretize than other finite difference methods. The development of the Crank-Nicolson model is included in Appendix B.

Table 4.1. Summary of system and biofilm model equations

System Model	$V_L \frac{dN}{dt} = -\frac{D_W}{L_L}(N_b - N_s) \times A_m \times {S_{SL}}^2$	Equation 4.13
Biofilm Model	$A(x)\frac{\partial N}{\partial t} = D_B \frac{\partial}{\partial x}\left(A(x)\frac{\partial N}{\partial x}\right) - A(x)\frac{\mu_m N}{K_N + N}\frac{X}{Y}$	Equation 4.29
Area as a Function of x	$A(x) = \frac{A_m \times (S_{SA} - 1)}{L}x + A_m$	Equation 4.19
Ammonia-N Utilization	$k = \frac{\mu_m}{Y}$	Equation 4.30
Biomass Volatile Density	$X = \frac{B \times VS}{L_a}$	Equation 4.40
Boundary Condition 1	$D_B \frac{dN}{dx}\Big\|_{x=0} = 0$	Equation 4.32
Boundary Condition 2	$D_B \frac{dN}{dx}\Big\|_{x=L} = -\frac{D_W}{L_L}(N_b - N_s)$	Equation 4.34

A(x) = biofilm diffusional area as a function of x (m^2)
A_m = media surface area in reactor (m^2)
B = biomass per unit area (g/m^2)
D_B = effective ammonia-N diffusion coefficient in the biofilm (m^2/d)
D_W = ammonia-N diffusion coefficient in water (m^2/d)
k = maximum specific ammonia-N utilization rate (g-N/g-VS/d)
K_N = ammonia-N half-saturation concentration ($g\text{-}N/m^3$)
L = biofilm thickness (m)
L_a = apparent biofilm thickness (m)
L_L = thickness of stagnant liquid layer (m)
N = ammonia-N concentration ($g\text{-}N/m^3$)
N_b = bulk liquid ammonia-N concentration ($g\text{-}N/m^3$)
N_s = ammonia-N concentration at liquid-biofilm interface ($g\text{-}N/m^3$)
S_{SA} = specific biofilm surface area (m^2/m^2)
t = time (d)
V_L = liquid volume in reactor (m^3)
VS = volatile solids percentage of biomass (%)
x = distance into biofilm (m)
X = volatile biomass density ($g\text{-}VS/m^3$)
Y = ammonia-N yield coefficient (g-VS/g-N)
μ_m = maximum specific growth rate (d^{-1})

Combining the Crank-Nicolson Method with the Complex Method of Constrained Optimization (Complex Method) results a systematic approach for solving the model. The Complex Method is in iterative process for optimizing functions of several variables that are known to lie within some constraining limits. The main idea is to test multiple potential solution vectors (each solution vector contains a potential solution for each variable) and adjust the worst vector. By continually adjusting the worst vector, this technique slowly converges upon the optimum solution. In order to properly use the Complex Method, there must by two or more potential solution vectors than then number of variables being optimized. The vector adjustment procedure involves relocating the worst solution vector through colocation with the centroid of the other potential solution vectors. This adjustment process continually moves are reshapes the boundary in which the optimum solution lies (Box, 1965).

To solve the model in this study, the Crank-Nicolson Method will be used to test potential solutions against the bench-scale trials and the Complex Method will be used to adjust potential solutions until convergence upon the optimum solution is achieved. The potential solutions will be compared to the observed data from the bench-scale trials be determining the R^2 value (as discussed in Section 4.1). This procedure will be iterated until the maximum R^2 value is achieved, thus resulting in the optimum solution for each bench-scale trial. In summary, the steps for solving for each bench-scale trial is as follows:

1. Input constants not affected by temperature (Y and L_L);
2. Determine and input constants affected by temperature (D_W and D_B) based on the temperature condition of the bench-scale trial;
3. Load the bench-scale trial specific parameters (L_a, L, S_{SA}, X, and V_L) based on the bench-scale trial; and

4. Use the Crank-Nicolson and Complex Method iterative approach to solve and determine the variable parameters (μ_m, K_N, and N_{b0}) for this bench-scale trial being tested.

The model parameters required to solve the unsteady-state model can be grouped into four categories as outlines in Table 4.2. The "constants not affected by temperature" include the yield coefficient and thickness of the stagnant liquid layer. Assumptions have been made regarding their values, as described in the model development, and the same values are used regardless of the bench-scale trial or the water temperature. The "constants affected by temperature" include the ammonia-N diffusion coefficients in water and in the biofilm and depend on the temperature but do not change between bench-scale trials of like temperature. The "bench-scale trial specific parameters" include the apparent biofilm thickness, the biofilm thickness based on truncated pyramid approximation, the specific biofilm surface area, and the biomass density. The values are specific to each bench-scale trial. The final model parameter category is the "variable parameters" and includes the maximum specific growth rate, the half-saturation concentration, and the initial bulk concentration. The "variable parameters" are the parameters that will be used in the combined Crank-Nicolson Method and Complex Method to iterate until the best solution is obtained.

Temperature impacts to the Monod kinetic parameters are commonly modeled by an Arrhenius-type relationship as shown previously in Equation 2.8. This type of equation correlates the kinetic parameter values at a 20°C to the kinetic parameter values other temperatures using a temperature activity coefficient. Equation 2.8, shown again as Equation 4.41, represents the Arrhenius-type relationship commonly used. The use of this type of equation for modeling the temperature impacts to the maximum specific growth rate (μ_m) and the

ammonia-N half-saturation concentration (K_N) will be explored as part of the research effort. Because the yield coefficient (Y) is assumed constant, the same relationship for the maximum specific growth rate (μ_m) will apply to the maximum ammonia-N utilization rate (k).

Table 4.2. Unsteady-state model parameters

Parameter	Value
Constants not affected by temperature	
Yield coefficient (Y)	0.25 g-VS/g-N
Stagnant liquid layer thickness (L_L)	40 μm
Volatile solids percentage of biomass (VS)	40 %
Constants affected by temperature	
Ammonia-N diffusion coefficient in water (D_W)	1.1×10^{-4} – 1.4×10^{-4} m^2/d
Effective ammonia-N diffusion coefficient in biofilm (D_B)	$0.6 \times D_W$
Bench-scale trial specific parameters	
Biofilm thickness (L and L_a)	Based on bench-trial data
Specific biofilm surface area (S_{SA})	Based on bench-trial data
Biomass density (X_T)	Based on bench-trial data
Liquid volume in reactor (V_L)	Based on bench-trial data
Variable parameters	
Maximum specific growth rate (μ_m)	TBD*
Ammonia-N half-saturation concentration (K_N)	TBD*
Bench-trial initial bulk ammonia-N concentration (N_{b0})	TBD*

* To be determined from solving the unsteady-state model

$$K_{T2} = K_{T1} \times \theta_K^{T2-T1} \quad (4.41)$$

K_{T1} = kinetic parameter at T1 °C (d^{-1})

K_{T2} = kinetic parameter at T2 °C (d^{-1})

θ_K = temperature-activity coefficient for parameter k

CHAPTER 5. RESULTS AND DISCUSSION

The results of this study pertaining to the temperature impacts to nitrification kinetics are contained within this chapter, and generally include discussions related to the unsteady-state model results, the biofilm characteristics analysis, and overall conclusions and recommendations. Results of the unsteady-state model and the impacts of temperature on Monod kinetics (the second and third research goals) are addressed in Section 5.1. The biofilm characteristics analysis is provided in Section 5.2 (addressing the first research goal) and includes analysis of trends between different biofilm parameters and potential relationships between biofilm parameters and water temperature. Overall conclusions of this research effort and recommendations for future research are contained within this chapter and are provided in Section 5.3.

5.1. Unsteady-State Model Results and Discussions

The unsteady-state model was solved using the results of the 12 bench-scale trials by minimizing the coefficient of determination (R^2) between the modeled and the observed bulk ammonia-N concentration. Solving was done following the methodology presented in Section 4.3. A summary of the biofilm characteristics required for solving the model for each bench-scale trial are presented in Table 5.1. The water temperature (T) and the unit biomass (B) were measured as discussed in Section 3.2, and the remaining parameters in Table 5.1 were calculated as described throughout Chapter 4. Additionally, a list of assumptions for key parameters is shown in Table 5.2.

Table 5.1. Biofilm characteristics from bench-scale trials

#	T [a] (°C)	B [b] (g-TS/m^2)	X_T [c] (kg/m^3)	L_a [d] (µm)	SSL [e] (m/m)	SSA [f] (m^2/m^2)	L [g] (µm)
1	20	7.51	119.4	62.90	2.20	4.84	23.47
2	20	7.39	117.4				
3	19	7.46	108.5	68.70	2.10	4.41	27.44
4	19	7.40	107.6				
5	15	6.88	129.5	53.10	2.40	5.76	17.39
6	16	7.26	136.6				
7	14	9.66	93.6	103.20	2.80	7.84	26.60
8	15	9.83	95.3				
9	11	14.35	93.3	153.70	3.40	11.56	28.89
10	11	14.11	91.8				
11	10	18.67	86.3	216.30	3.70	13.69	35.29
12	10	18.87	87.2				

[a] T is the water temperature (°C)

[b] B is the unit biomass (g-TS/m^2)

[c] X_T is the biomass density (g-TS/m^3)

[d] L_a is the apparent biofilm thickness [based on the image analysis] (µm)

[e] S_{SL} is the specific surface length (m/m)

[f] S_{SA} is the specific surface area (m^2/m^2)

[g] L is the biofilm thickness [based on the truncated pyramid approximation] (µm)

Table 5.2. Key unsteady-state model parameter assumptions

Parameter	Value
Yield coefficient (Y)	0.25 g-VS/g-N
Stagnant liquid layer thickness (L_L)	40 µm
Volatile solids percentage of biomass (VS)	40 %
Effective ammonia-N diffusion coefficient in biofilm (D_B)	0.6 × D_W*

* D_W is the ammonia-N diffusion coefficient in water and ranges from 1.1×10^{-4} to 1.4×10^{-4} m^2/d depending on the water temperature (Stewert, 2003)

The solutions of the unsteady-state model for each bench-scale trial are shown in Table 5.3 and the individual results for each trial are shown graphically in Figure 5.1 through Figure 5.6. The figures compare the modeling results with the observed results during the bench-scale trials. From the figures, it is evident that the unsteady-state model fits the bench-scale trial results quite well with the lowest R^2 value among the trials equaling 0.9955 for trial 1.

Table 5.3. Unsteady-state model results for the bench-scale trials

			Calculated Parameters			
#	T [a] (°C)	Duration (min)	N_{b0} [b] (mg-N/L)	μ_m [c] (day^{-1})	k [d] (g-N/g-VS-d)	K_c [e] (mg-N/L)
1	20	330	33.9	0.061	0.243	2.27
2	20	330	36.5	0.069	0.277	3.09
3	19	225	27.3	0.070	0.280	1.28
4	19	210	24.6	0.080	0.320	2.48
5	15	195	13.1	0.051	0.205	1.92
6	16	180	14.5	0.049	0.194	1.26
7	14	225	24.6	0.047	0.189	1.58
8	15	225	32.9	0.051	0.204	0.01
9	11	180	19.5	0.027	0.107	0.65
10	11	180	18.7	0.026	0.104	0.37
11	10	300	38.1	0.028	0.113	3.55
12	10	255	30.0	0.026	0.106	4.05

[a] T is the water temperature (°C)

[b] N_{b0} is the initial ammonia-N concentration (mg-N/L)

[c] μ_m is the maximum specific growth rate ($days^{-1}$)

[d] k is the ammonia-N maximum specific utilization rate (g-N/g-VS-d) and is equal to μ_m/Y

[e] K_c is the ammonia-N half-saturation concentration (mg-N/L)

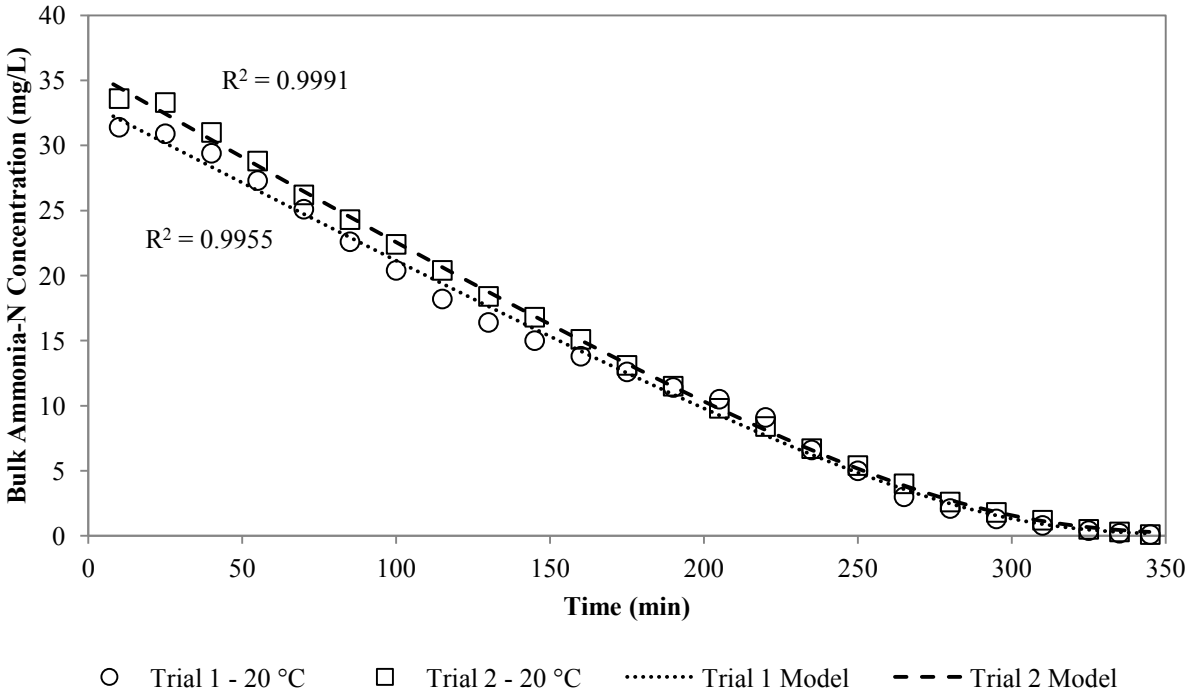

Figure 5.1. Model of bench-scale trials 1 and 2 (20°C)

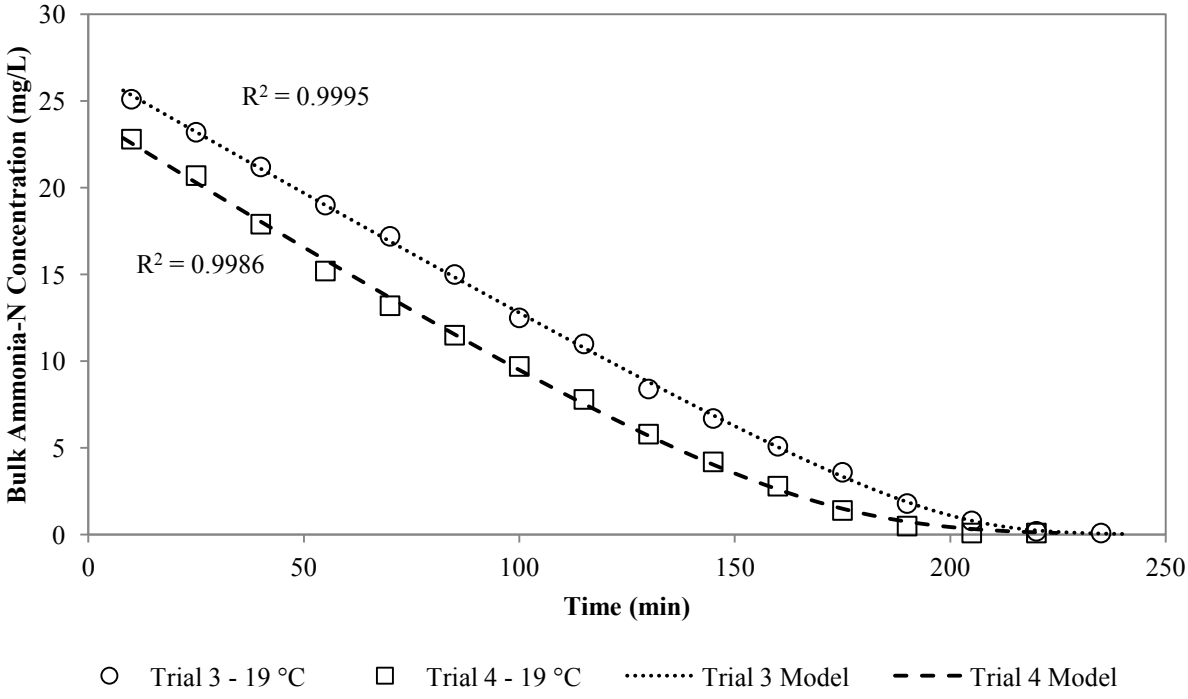

Figure 5.2. Model of bench-scale trials 3 and 4 (19 °C)

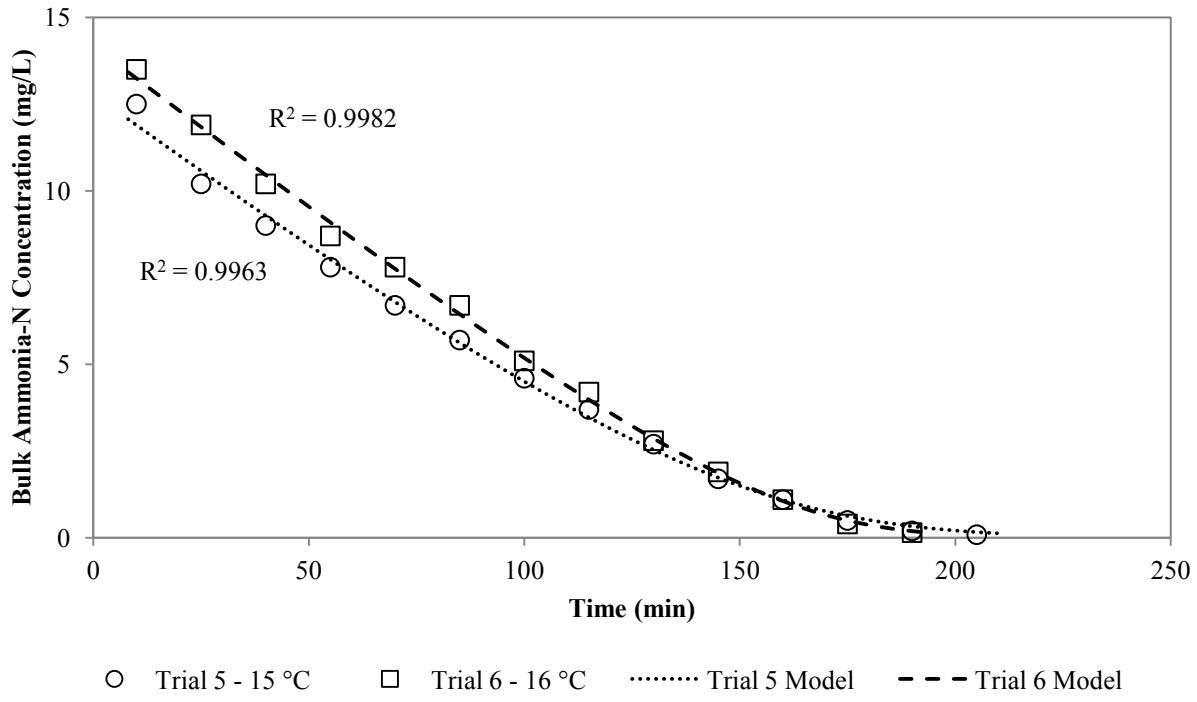

Figure 5.3. Model of bench-scale trials 5 and 6 (15/16 °C)

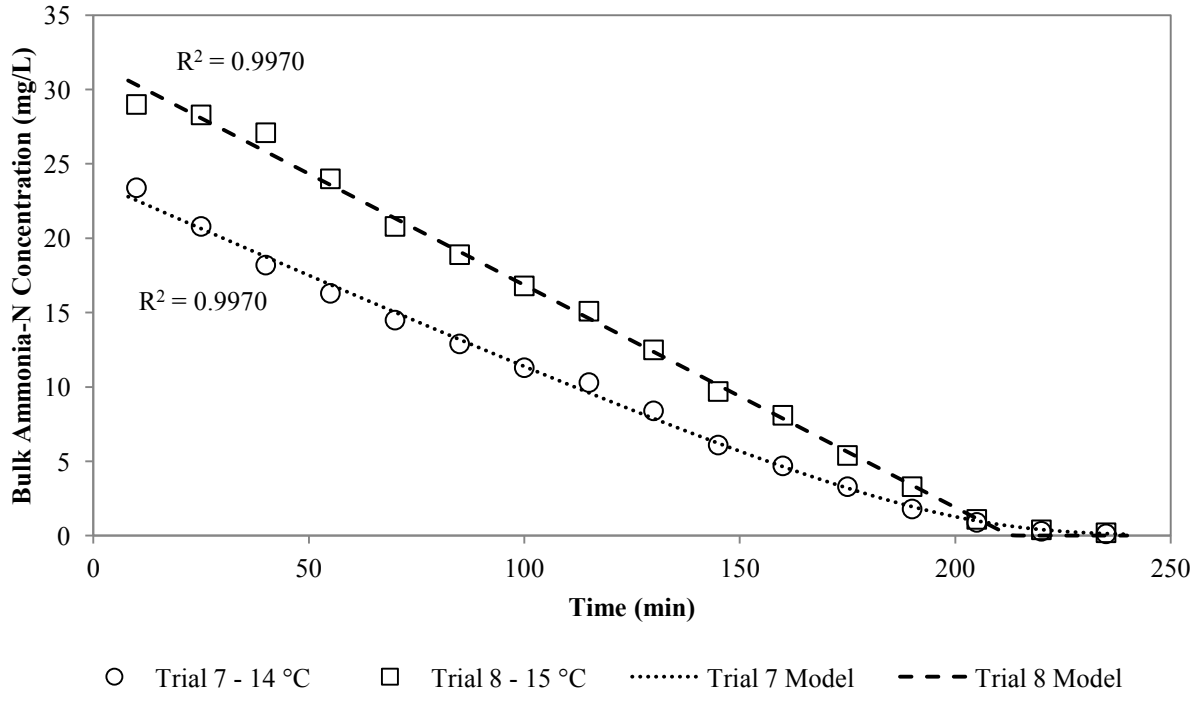

Figure 5.4. Model of bench-scale trials 7 and 8 (14/15 °C)

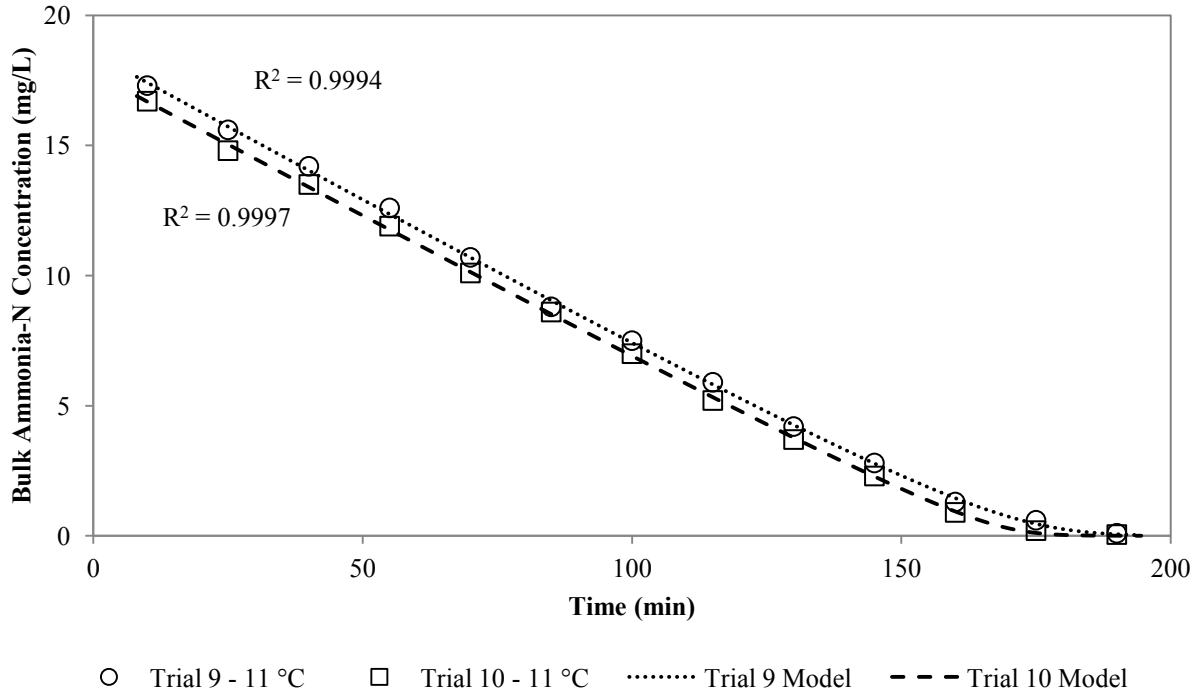

Figure 5.5. Model of bench-scale trials 9 and 10 (11 °C)

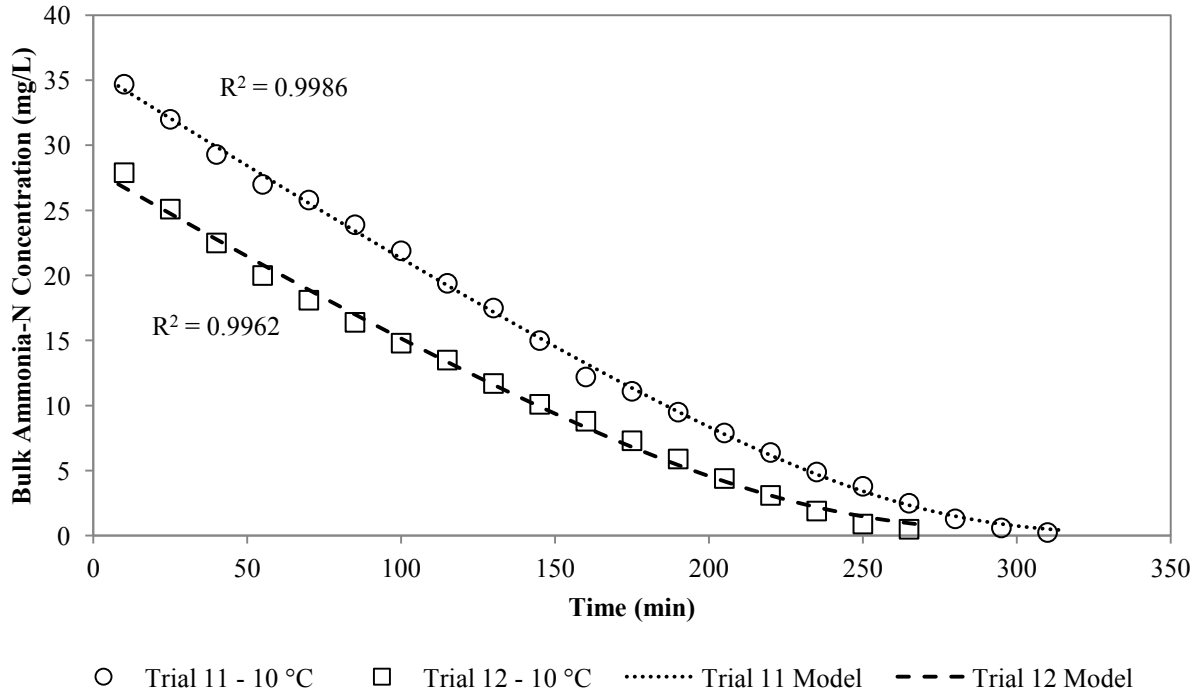

Figure 5.6. Model of bench-scale trials 11 and 12 (10 °C)

Because the unsteady-state model fits the bench-scale trial results very well, the results of the unsteady-state model can be used to study the impacts of temperature on nitrification kinetics. A plot of the maximum specific growth rate (μ_m) versus temperature and the ammonia-N half-saturation concentration (K_N) versus temperature is shown as Figure 5.7. The figure indicates that the maximum specific growth rate increases exponentially with increasing temperature. This relationship follows the Arrhenius-type relationship presented as Equation 2.8. From the relationship determined from the unsteady-state modeling, the equation for the maximum specific growth rate as a function of temperature is shown as Equation 5.1, with a $\mu_{m,20}$ of 0.147 $days^{-1}$ and a θ_μ value of 1.097. This relationship has a strong R^2 value of 0.8711 thus indicating the applicability of the Arrhenius-type relationship for modeling the temperature impacts to the maximum specific growth rate. The values for μ_m and for $\mu_{m,20}$ are slightly below the range of reference values shown in Table 2.1, while the θ_μ value falls within the range of reference values from Table 2.2. The values for the maximum specific growth rate are slightly low because the entire volatile biomass density was used in the model; however, as discussed in Section 2.3, only the ammonia oxidizing bacteria (AOB) contribute to nitrification and the AOB only occupies a fraction of the volatile solids. Using the entire volatile biomass in the modeling is preferable from a laboratory setting due to the ease of determining the volatile solids percentage.

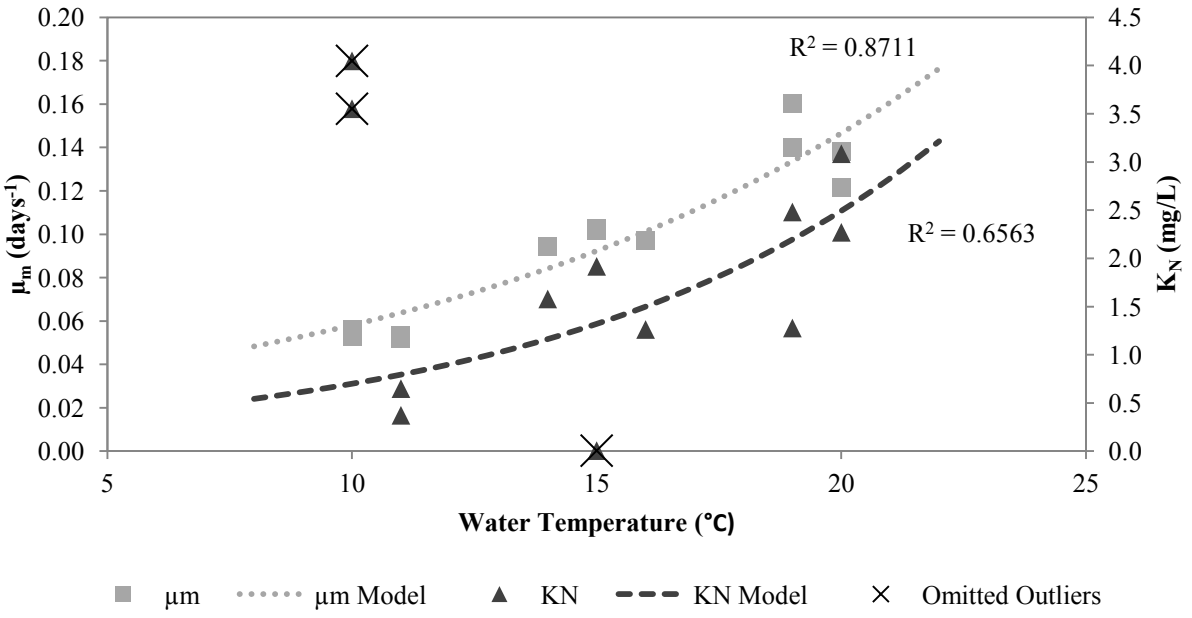

Figure 5.7. Diffusion model determined kinetics parameters (μ_m and K_N) versus temperature

$$\mu_m = \mu_{m,20} \times \theta_\mu^{(T-20)} = 0.0733 \times 1.097^{(T-20)} \quad (5.1)$$

μ_m = maximum specific growth rate ($days^{-1}$) at temperature T

$\mu_{m,20}$ = maximum specific growth rate ($days^{-1}$) at 20 °C

θ_μ = temperature-activity coefficient for μ_m

T = temperature (°C)

The half-saturation concentration value is important at defining the curvature of bench-scale ammonia-N removal plots, especially at lower temperatures. From analyzing the relationship between the ammonia-N half-saturation concentration (K_N) from Figure 5.7 indicates that the ammonia-N half-saturation concentration also increases exponentially with increasing temperature. Upon closer examination of results for bench-scale trials 8, 11, and 12,

it can be concluded that not enough samples were taken at low ammonia-N concentrations to adequately model the half-saturation concentration. Removal of these apparent outliers, as shown in Figure 5.7, yields a stronger relationship ($R^2 = 0.6563$) between the half-saturation concentration and temperature. The resulting Arrhenius-type relationship is shown as Equation 5.2, with $K_{N,20}$ equaling 2.49 mg/L as ammonia-N and a θ_K value of 1.136. The $K_{N,20}$ value is higher than the reference values from Table 2.1; however, most reference cited in the table had assumed values for K_N. Values for θ_K for fixed film systems are not well understood or documented.

$$K_N = K_{N,20} \times \theta_K{}^{(T-20)} = 2.49 \times 1.136^{(T-20)} \quad (5.2)$$

K_N = maximum specific growth rate (mg-N/L) at temperature T

$K_{N,20}$ = maximum specific growth rate (mg-N/L) at 20 °C

θ_K = temperature-activity coefficient for K_N

Another observation of the model is the ammonia-N profile through the biofilm. It was found that the ammonia-N concentration fully penetrated the biofilm for all bench-scale trials and temperature conditions. In fact, the ammonia-N concentration was only slightly less at the biofilm interface with the media as it was at the surface of the biofilm. This fact, gives rise to the idea that a fixed film system with a relatively thin biofilm could be modeled similar to a suspended growth system and nitrification kinetics for fixed film systems with thin biofilm is not controlled by diffusion into the biofilm.

Overall, the unsteady-state model was able to successfully simulate the results of the bench-scale trials. The impacts of temperature on the kinetic rates can be effectively modeled

with the conventional Arrhenius-type relationships (a summary of the kinetic parameters from the diffusion model is shown below in Table 5.4). However, as discussed in the following section, the changes in biofilm characteristics play a key role in the success of the unsteady-state model and are a significant reason for the unhindered performance of fixed film processes experiencing cold water temperatures.

Table 5.4. Fixed film nitrification kinetic parameter summary

Parameter	Value at 20 °C	Temperature-Activity Coefficient (θ)
Maximum specific growth rate (μ_m)	0.147 $days^{-1}$	1.097
Ammonia-N half-saturation concentration (K_c)	2.49 mg-N/L	1.136
Yield coefficient (Y)*	0.25 g-VS/g-N	1.000

* The values for the yield coefficient were assumed

5.2. Biofilm Characteristics Trend Analysis

A biofilm characteristics trend analysis was performed as part of this research effort. This was done in order to better understand how biofilm parameters react to changes in water temperature and with changes in the amount of attached biomass. Because of their use in the unsteady-state model, parameters of key interest include biomass per unit area, specific biofilm surface area, biofilm thickness, and biomass density. Potential correlations between these biofilm parameters and water temperature are explored in the following sections along with understanding of how these parameters affect the overall nitrification performance.

As part of previous studies of the full-scale Moorhead MBBR, significant sampling in addition to the bench-scale trial has been performed and involved biomass per unit area sampling and detailed image analysis. Comparatively, the biomass per unit area sampling is much less

intensive than the image analysis. Therefore, models that could be used to predict biofilm parameters in lieu of the image analysis are essential in future study of fixed film processes.

5.2.1. Temperature Impacts on Biomass

In a previous study of the Moorhead MBBR, a correlation between the amount of biomass in the MBBR and the water temperature was observed. The correlation between the historical biomass per unit area and water temperature is shown in Figure 5.8. The figure also shows the biomass per unit area corresponding to when active media was taken from the full-scale MBBR to perform the bench-scale trials. There is a very obvious inverse correlation between the biomass per unit area and the temperature indicating that more biomass is present at colder water temperatures (Bjornberg et al., 2010). It should be noted that one apparent outlier indicated in Figure 5.8 has been omitted from further analysis.

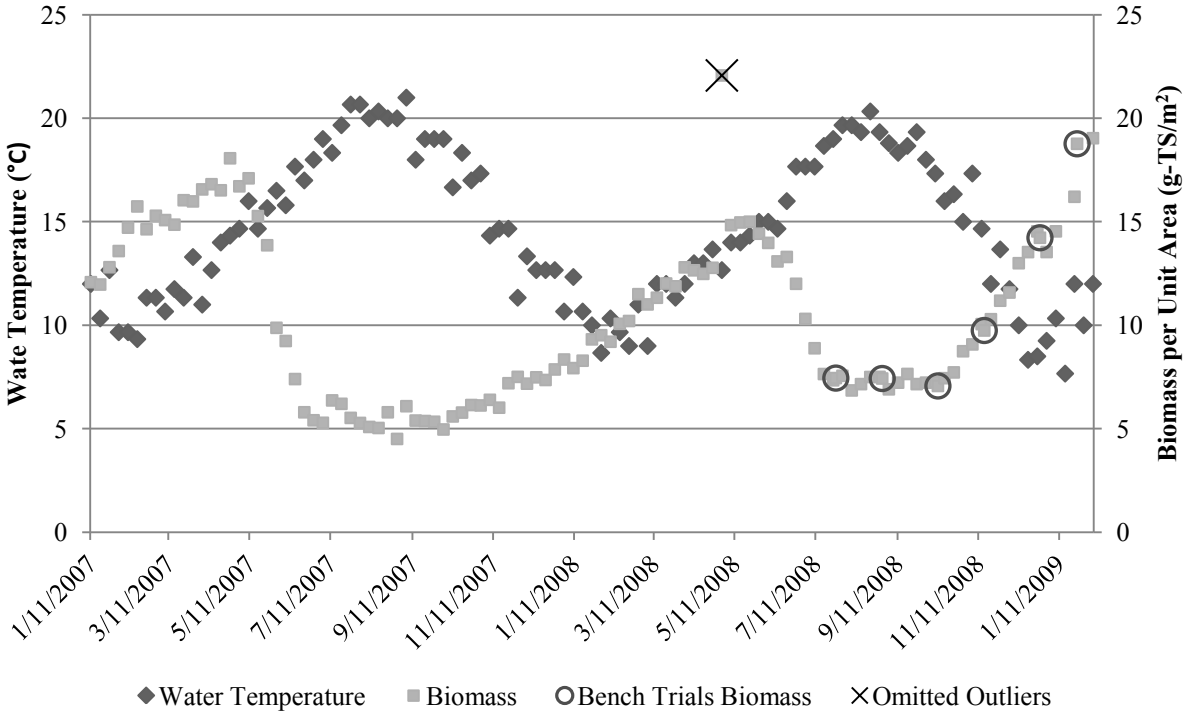

Figure 5.8. Historical temperature and biomass per unit area (Source: Bjornberg et al., 2010)

From Figure 5.8, it is evident that water temperature in the Moorhead MBBR gradually changes in response to ambient temperature. This follows typical wastewater temperature trends, where the water temperature is regulated due to the addition of warm water from households and industrial users, and temperature changes are slow and in reaction to seasonal variations (Metcalf & Eddy, 2003). This observation is important because it explains why more biomass is present at colder temperatures. First, the gradual temperature changes allow sufficient time for the slow-growing nitrifying biomass to adjust to the temperatures changes. Secondly, due to decreased kinetic rates at colder temperatures as previously demonstrated, an equal ammonia-N loading rate can support a larger biomass population at colder temperatures. Therefore, at colder temperatures following a gradually adjustment, the biomass has had time to adjust and more biomass is present. This observation can be expanded to all fixed film wastewater treatment processes because wastewater does not typically experience sudden temperature changes, and it is unlikely that typically domestic wastewater treatment plants experience water temperature colder than the Moorhead MBBR.

5.2.2. Relationship between Biomass and Water Temperature

The first biofilm parameter relationship explored was between the biomass per unit area (B) and water temperature (T). The relationship was analyzed using the 112 samples shown in Figure 5.8. The resulting relationship, Figure 5.9, shows the trend in average biomass per unit area measurements at different temperature and the corresponding variation. From the figure, it is evident that the biomass per unit area decreases exponentially with an increase in temperature. Also, the data indicates more variability at colder temperatures, with the widest variability seen between approximately 12 and 16 °C. It was noted by Bjornberg (2009) that significant changes

in biomass occurred during sloughing or growth events that occurred around approximately these temperatures. This observation can help to explain the increased variability in biomass per unit area at these water temperatures.

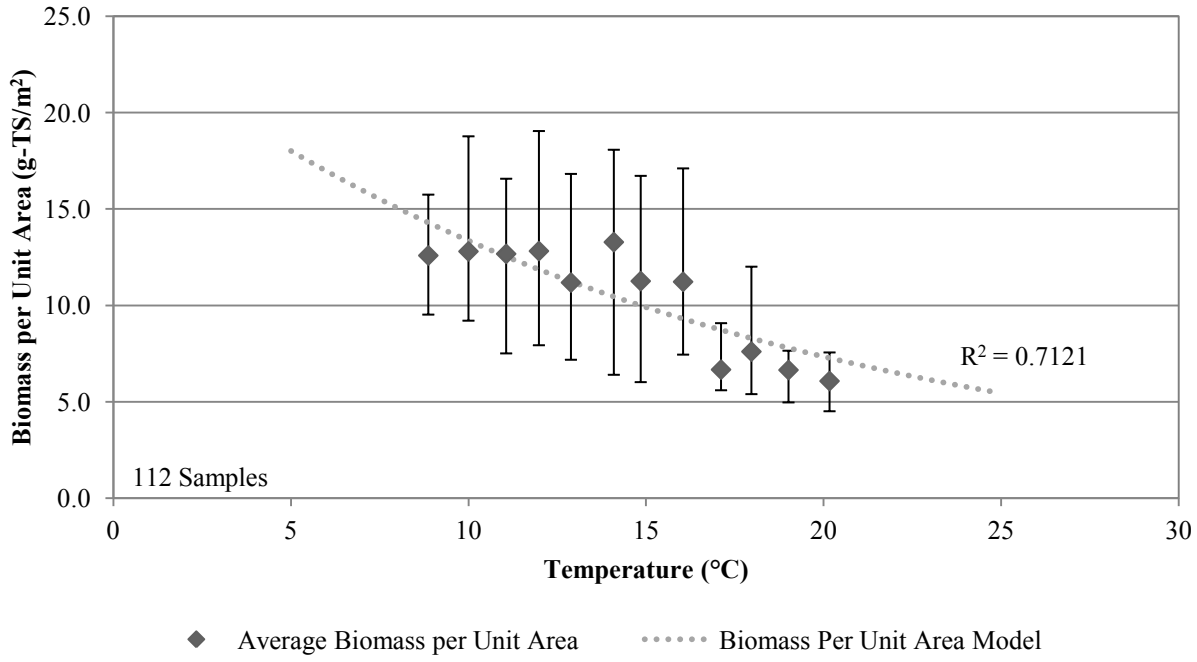

Figure 5.9. Average biomass per unit area (B) versus water temperature (T)

Equation 5.3 was developed to predict the average biomass per unit area (B) as an exponential function of water temperature (T). This relationship is shown graphically in Figure 5.9. The R^2 value for the relationship between the average biomass per unit area and the water temperature is 0.7121; however, there is some variability within the data but the general shape of the data follows the trend.

$$B = 24.3 \times e^{-0.0598 \times T} \tag{5.3}$$

B = biomass per unit area (g-TS/m^2)

T = water temperature (°C)

5.2.3. Relationship between Biofilm Surface Area and Biomass

The next relationship explored was between the biofilm surface area and biomass. It was found that the specific biofilm surface area (S_{SA}) shows strong linear correlation with the biomass per unit area (B) as indicated in Figure 5.10. Equation 5.4 was developed to model this relationship. The intercept was set equal to 1.0 indicating that when no biomass is present the specific surface area is equal to 1.0 and therefore the biofilm surface area is equal to the media surface area in the reactor (A_m). The equation for the specific surface area as a function of the biomass per unit area is a good fit for the observed data with an R^2 value of 0.7265. This relationship indicates that when more biomass is present (as result of declining temperature) the biofilm surface area linearly increases. It should be noted that the specific surface area is the square of the specific surface length (S_{SL}) that was actually measured. If needed, equations for the specific surface length could be determined by taking the square root of the specific surface area.

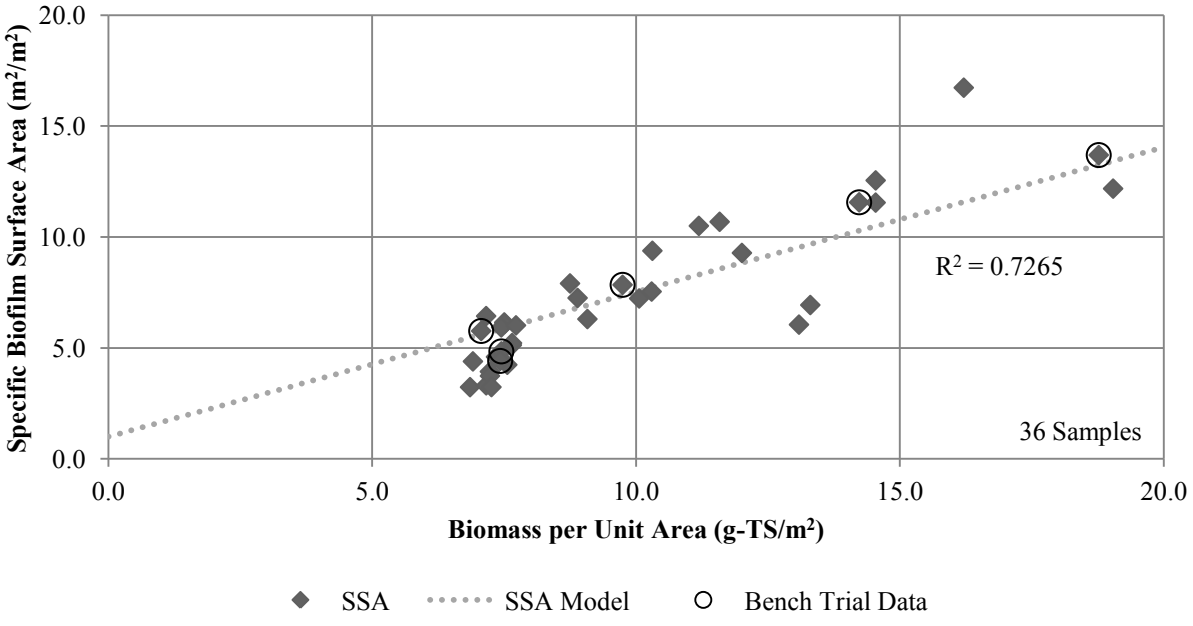

Figure 5.10. Specific biofilm surface area (S_{SA}) versus biomass per unit area (B)

$$S_{SA} = {S_{SL}}^2 = 0.652 \times B + 1 \quad (5.4)$$

S_{SA} = specific surface area (m^2/m^2)

S_{SL} = specific surface length (m^2/m^2)

5.2.4. Relationship between Biofilm Thickness and Biomass

The biofilm thickness is an important parameter needed in the unsteady-state model, and as shown during the model development, the biofilm thickness is treated as two related parameters: (1) the apparent biofilm thickness (L_a) that is measured and determined from the image analysis, and (2) the biofilm thickness (L) that is calculated based on the truncated pyramid approximation. Equation 4.3 and Equation 4.9 indicate that the biofilm thickness (L) is a function of the apparent biofilm thickness (La) and the specific surface area (S_{SA}) (and consequently a function of the specific surface length (S_{SL})). These parameters are all interconnected, shown as Equation 5.5, and it is ideal to explore mathematical relationships that utilize the interconnection.

$$L = \frac{3 \times L_a}{\left(1 + \sqrt{S_{SA}} + S_{SA}\right)} = \frac{3 \times L_a}{\left[1 + \sqrt{0.652 \times B + 1} + (0.652 \times B + 1)\right]} \quad (5.5)$$

L_a = apparent biofilm thickness (μm)

Because the apparent biofilm thickness (L_a) was measured as part of the image analysis, it was decided that potential relationships between thickness and biomass should be based on the apparent thickness. Equations for the biofilm thickness (L) can then be derived using Equation

5.5. As such, the relationship between the apparent biofilm thickness (L_a) and the biomass per unit area (B) was explored, with the result shown in Figure 5.11. From the figure, there is a positive correlation between the apparent biofilm thickness and the biomass per unit area.

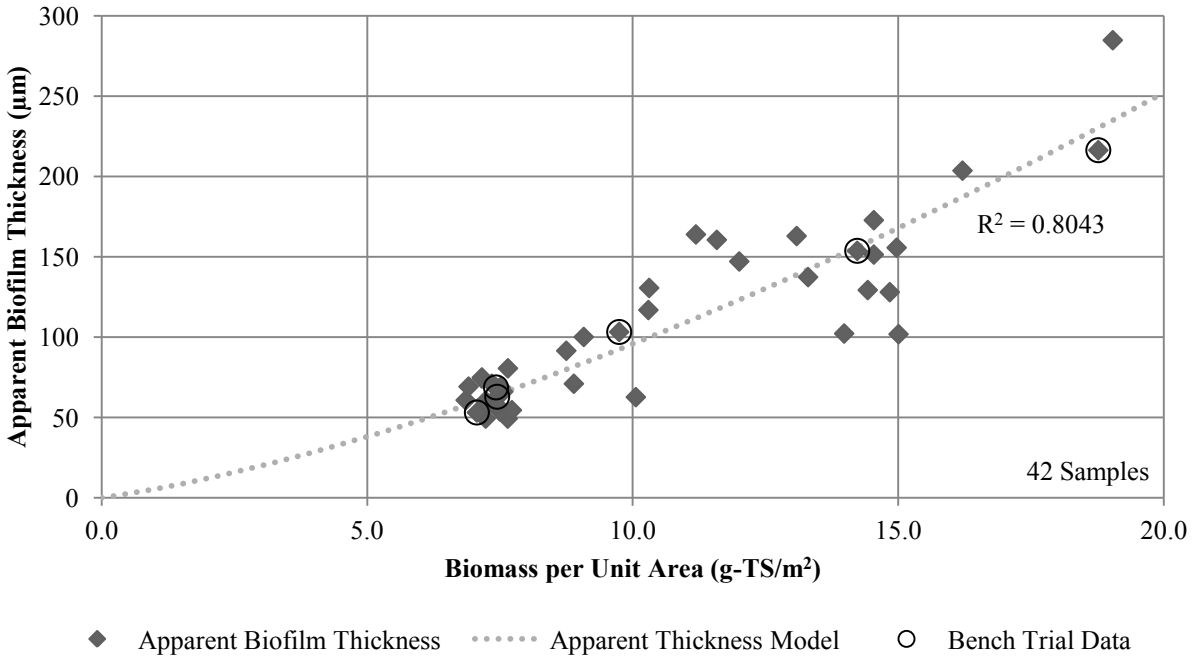

Figure 5.11. Apparent biofilm thickness (L_a) versus biomass per unit area (B)

After fitting the data, the equation for apparent biofilm thickness as a function of the biomass per unit area is shown as Equation 5.6, with an R^2 value of 0.8043 indicating a good fit. The equation indicates that the apparent biofilm thickness increases as a function of the biomass per unit area raised to the 3/2 power, meaning the biofilm is thicker when more biomass is present. The equation also implies that when no biomass is present the apparent biofilm thickness is zero. Because of the interconnection between these parameters, Equation 5.6 can be written in terms of the specific surface area as shown.

$$L_a = 4.88\left[(0.652 \times B + 1)^{3/2} - 1\right] = 4.88\left({S_{SA}}^{3/2} - 1\right) \quad (5.6)$$

L_a = apparent biofilm thickness (μm)

The form of Equation 5.6 was chosen to take advantage of the parameter interconnectivity, and essentially aimed at ensuring that Equation 5.5 held true as well as providing algebraic simplification. By combing Equations 5.5 and Equation 5.6, Equation 5.7 for the biofilm thickness (L) is derived. The equation also shows the algebraic simplification that can be performed because of the consideration taken while developing Equation 5.6. Further simplification of the relationship results in Equation 5.8, which correlates the biofilm thickness to the biomass per unit area. Similar to the apparent biofilm thickness, the equations indicate that the biofilm thickness increases when more biomass is present (due to decreasing water temperatures).

$$L = \frac{3 \times 4.88\left({S_{SA}}^{3/2} - 1\right)}{\left(1 + \sqrt{S_{SA}} + S_{SA}\right)} = \frac{3 \times 4.88\left(\sqrt{S_{SA}} - 1\right)(1 + \sqrt{S_{SA}} + S_{SA})}{\left(1 + \sqrt{S_{SA}} + S_{SA}\right)} = 3 \times 4.88\left(\sqrt{S_{SA}} - 1\right) \quad (5.7)$$

$$L = 3 \times 4.88\left(\sqrt{S_{SA}} - 1\right) = 14.64\left[(0.652 \times B + 1)^{1/2} - 1\right] \quad (5.8)$$

L = biofilm thickness (μm)

5.2.5. Relationship between Biomass Density and Biomass

To conclude the biofilm characteristics trend analysis, relationships involving the total biomass density (X_T) were developed. Similar to the biofilm thickness (L), the total biomass density is a calculated parameter that is based on equations previously developed. Equation 5.9,

developed by combining Equation 4.39 and Equation 4.40, relates the biomass density to the biomass per unit area (B) and to the apparent biofilm thickness (L_a). As shown, substitution of Equation 5.6 modifies the equation for the biomass density into a function of only the biomass per unit area. This relationship as well as the observed data is shown in Figure 5.12. Equation 5.9 provides a relatively good fit of the data; however, it should be noted that much of the variability seen within the figure is caused by the variation within the biomass per unit area data previously discussed. Overall, this relationship indicates that the total biomass density declines as the amount of biomass increases as results of decreasing water temperature.

$$X_T = \frac{B}{L_a} = \frac{0.205 \times B}{(0.652 \times B + 1)^{3/2} - 1} \tag{5.9}$$

X_T = total biomass density (g/m^3)

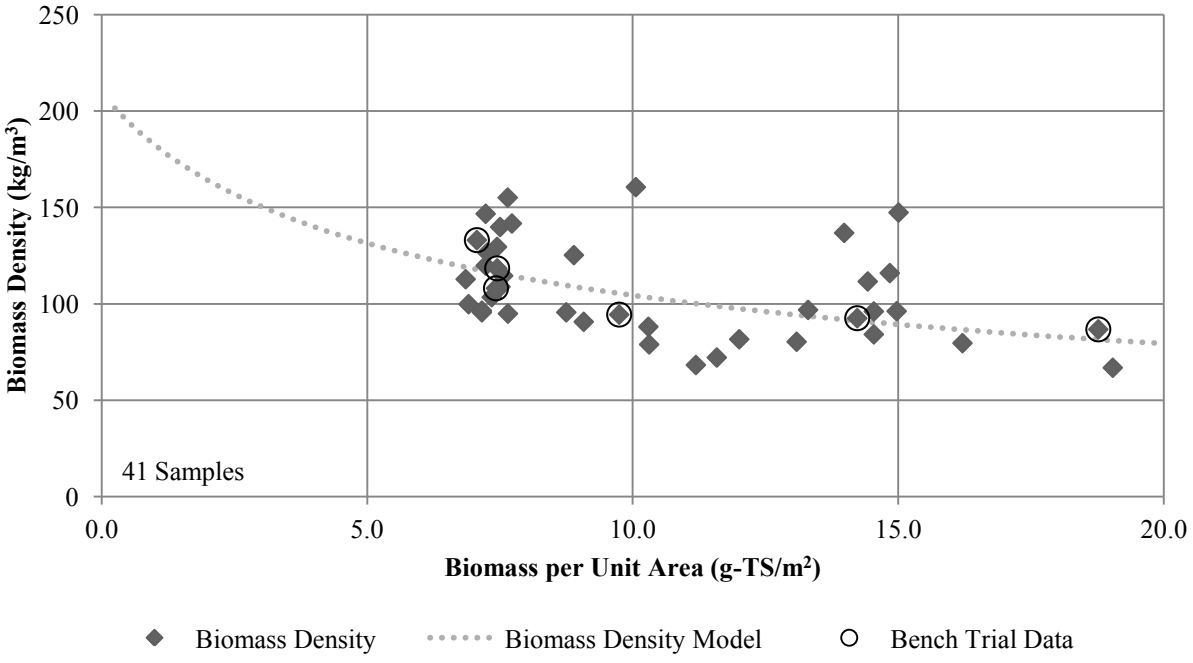

Figure 5.12. Biomass density (X_T) versus biomass per unit area (B)

As noted previously, the effective diffusion coefficient in the biofilm considers density and the observed changes in biomass density could warrant a density dependent diffusion coefficient. However, for thin biofilms, like that of the Moorhead MBBR, it was found that diffusion does not govern the nitrification process and a density dependent effective diffusion coefficient may be more applicable for thick biofilm systems.

5.3. Conclusions and Recommendations

The results of the unsteady-state model simulations of the bench trial results conclude that the maximum specific growth rate (μ_m) and ammonia-N half-saturation concentration (K_N) decreased with declining temperature. This indicates that nitrification kinetics for full-scale fixed film systems are affected by temperature and the conventionally understood Monod kinetics and temperature correction factors do apply.

The biofilm characteristics trend analysis aimed to determine how the biomass changes as result of gradual changes in water temperature. Colder water temperatures support more nitrifying biomass due to declining kinetic rates, as indicated by the observed increase in biomass per unit area. Furthermore, the increase in biomass per unit area prompted additional changes in the biomass, specifically, the biofilm surface area increases, the biofilm thickness increases, and the biomass density decreases. Equations used to model these changes in biofilm characteristics as a function of the temperature or of the biomass per unit area measurements were developed. The equations were reasonable predictors of the observed data; however, variations within the biomass per unit area measurement did show through into the relationships with other parameters and additional investigation may be warranted. The equations will be useful for modeling fixed film wastewater treatment processes because they predict biofilm

characteristics as a function of water temperature and are important to explaining the good cold weather performance of fixed film processes.

To expand on the biomass density observation, it was found that the biomass density decreased with an increase in biomass. This also corresponds to a decrease in biomass density at colder temperatures. As noted, diffusion did not limit the nitrification performance for fixed film processes for thin biofilms, such as the Moorhead MBBR; however, the change in biomass density could change the diffusional properties such as the effective diffusion coefficient for fixed film systems experiencing thicker biofilms. This would result in deeper substrate penetration at colder temperatures for thicker biofilms.

Overall, the unsteady-state based model and nitrification kinetics can fit the experimental data and work well for fixed film wastewater systems as long as consideration is given for changes in the biofilm characteristics due to changes in temperature. The Monod kinetic parameters obtained from each bench-scale trial were evaluated and the results indicate that the commonly used temperature correction method also works well. The increased biomass (Figure 5.9) present in colder conditions offset the effects of decreased kinetics and allow for unhindered performance of fixed-film systems in colder conditions. Therefore, to properly apply Monod nitrification kinetics to fixed film systems, both temperature impacts to kinetics and temperature impacts to biofilm characteristics have to be applied.

Based on the research presented in this document, additional opportunities are presented to further investigate the full-scale Moorhead MBBR and performance of fixed film wastewater treatment processes. Some of the ideas are geared at making improvements to the diffusion-based unsteady-state model developed herein, while other ideas are relate to better understanding

of key factors influencing fixed film treatment performance such as temperature. The ideas for future research that are recommended include:

- Incorporate dissolved oxygen (DO) and consideration for nitrate and nitrite into the unsteady-state model,
- Further investigation into the biomass makeup, specifically determining AOB and NOB fractions and how they change with temperature or other factors,
- Better understanding of the yield coefficient and how it relates to the various biomass components including AOB and NOB,
- Developed a simpler suspended growth type model for the fixed film systems experiencing thin biofilms to verify the unimportance of the diffusion component,
- Test the unsteady-state model and biofilm characteristics trends using a fixed film system with a thicker biofilm such as a trickling filter and determine how important diffusion is for thicker biofilms,
- Determine how loading rates affects biofilm growth and overall system performance,
- Continue to monitor and study the Moorhead MBBR to enhance the relationships between temperature, biomass, and biofilm characteristics, and
- Incorporate the temperature impacts to nitrification kinetics found herein into full-scale MBBR models and modeling software packages.

REFERENCES

Biesterfeld, S., Farmer, G., Russell, P., & Figueroa, L. (2001). Effect of Alkalinity Type and Concentration on Nitrifying Biofilm Activity. *Proceedings of the 74th Annual Water Environment Federation Technical Exhibition and Conference.* Atlanta, GA Oct. 13 - Oct. 17.

Bjornberg, C. (2009). *Effect of Temperature on Biofilm Growth Dynamics and Nitrification Kinetics in a Full-Scale Moving Bed Biofilm Reactor.* MS Thesis, North Dakota State University, Department of Civil Engineering, Fargo, ND.

Bjornberg, C., Lin, W., & Zimmerman, R. (2010). Kinetic Evaluation and Model Simulation of Temperature Impact on Biofilm Growth and Nitrification in a Full-Scale MBBR System. *Proceedings of the 83rd Annual Water Environment Federation Technical Exhibition and Conference.* New Orleans, LA, Oct. 2 - Oct. 6.

Boltz, J. P., Johnson, B. R., Daigger, G. T., & Sandino, J. (2009). Modeling Integrated Fixed-Film Activated Sludge and Moving-Bed Biofilm Reactor Systems I: Mathematical Treatment and Model Development. *Water Environment Research, 81*(6), 555-575.

Box, M. J. (1965). A new method of constrained optimization and a comparison with other methods. *The Computer Journal, 8*(1), 42-53.

Chen, S., Ling, J., & Blancheton, J.-P. (2006). Nitrification kinetics of biofilm as affected by water quality factors. *Aquacultural Engineering, 34*, 179–197.

City of Moorhead, MN. (2012). *Wastewater Treatment Facility.* Retrieved December 14, 2013, from http://www.ci.moorhead.mn.us/city_services/

Dinçer, A. R., & Kargı, F. (2000). Kinetics of sequential nitrification and denitrification processes. *Enzyme and Microbial Technology, 27*, 37-42.

Grady, C. P., Daigger, G. T., Love, N. G., & Filipe, C. D. (2011). *Biological Wastewater Treatment* (3rd ed.). Boca Raton, FL: CRC Press.

Göransson, E. (2004). *Low Order Approximations of Continuously Stirred Biofilm Reactors with Monod Kinetics.* Chalmers University of Technology, Control and Automation Laboratory Department of Signals and Systems, Göteborg, Sweden.

Henze, M., van Loosdrecht, M., Ekama, G., & Brdjanovic, D. (Eds.). (2008). *Biological wastewater treatment: principles, modelling and design.* IWA Publishing.

Houweling, D., Monette, F., Millette, L., & Comeau, Y. (2007). Modelling Nitrification of a Lagoon Effluent in Moving-Bed Biofilm Reactors. *Water Quality Research Journal of Canada, 42*(4), 284-294.

Katipoglu-Yazan, T., Cokgor, E. U., Insel, G., & Orhon, D. (2012). Is ammonification the rate limiting step for nitrification kinetics? *Bioresource Technology, 114*, 117-125.

Lin, Y.-H. (2008). Kinetics of nitrogen and carbon removal in a moving-fixed bed biofilm reactor. *Applied Mathematical Modelling, 32*, 2360-2377.

Melo, L. (2005). Biofilm physical structure, internal diffusivity and tortuosity. *Water Science & Technology, 52*(7), 77-84.

Meng, Q., & Ganczarczyk, J. (2004). Full scale comparison of heterotrophic and nitrifying RBC biofilms. *Environmental Technology, 25*(2), 165-171.

Metcalf & Eddy. (2003). *Wastewater Engineering Treatment and Reuse* (4th ed.). (G. Tchobanoglous, F. L. Burton, & H. D. Stensel, Eds.) New York, NY: McGraw-Hill.

Press, W. H., Flannery, B. P., Teukolsky, S. A., & Vetterling, W. T. (1986). *Numerical Recipes: The Art of Scientific Computing.* Cambridge University Press.

Regmi, P., Wes, T., Schafran, G., Bott, C., Rutherford, B., & Waltrip, D. (2011). Nitrogen removal assessment through nitrification rates and media biofilm accumulation in an IFAS process demonstration study. *Water Research, 45*, 6699-6708.

Rusten, B., Eikebrokk, B., Ulgenes, Y., & Lygren, E. (2006). Design and operations of the Kaldnes moving bed biofilm reactors. *Aquacultural Engineering, 34*(3), 322-331.

Salvetti, R., Azzellino, A., Canziani, R., & Bonomo, L. (2006). Effects of temperature on tertiary nitrification in moving-bed biofilm reactors. *Water Research, 40*, 2891-2993.

Seifi, M., & Fazaelipoor, M. H. (2012). Modeling simultaneous nitrification and denitrification (SND) in a fluidized bed biofilm reactor. *Applied Mathematical Modelling, 36*, 5603-5613.

Sen, D., & Randall, C. W. (2008). Improved Computational Model (AQUIFAS) for Activated Sludge, Integrated Fixed-Film Activated Sludge, and Moving-Bed Biofilm Reactor Systems, Part II: Multilayer Biofilm Diffusional Model. *Water Environment Research, 80*(7), 624-632.

Sin, G., Weijma, J., Spanjers, H., & Nopens, I. (2008). Dynamic model development and validation for a nitrifying moving bed biofilter: Effect of temperature and influent load on the performance. *Process Biochemistry, 43*, 384-397.

Stewert, P. S. (2003). Diffusion in Biofilms. *Journal of Bacteriology, 185*(5), 1485-1491.

Thalla, A. K., Bhargava, R., & Kumar, P. (2010). Nitrification kinetics of activated sludge-biofilm system: A mathematical model. *Bioresource Technology, 101*, 5827-5835.

WEF. (1998). *Biological and Chemical Systems for Nutrient Removal.* Alexandria, VA: Water Environment Federation.

Zhang, S., Wang, Y., He, W., Wu, M., Xing, M., Yang, J., Gao, N., Pan, M. (2014). Impacts of temperature and nitrifying community on nitrification kinetics in a moving-bed biofilm reactor treating polluted raw water. *Chemical Engineering Journal, 236*, 242-250.

Zhang, S., Wang, Y., He, W., Wu, M., Xing, M., Yang, J., Gao, N., Yin, D. (2013). Responses of biofilm characteristics to variations in temperature and NH4+-N loading in a moving-bed biofilm reactor treating micro-polluted raw water. *Bioresource Technology, 131*, 365-373.

Zhu, S., & Chen, S. (2002). The impact of temperature on nitrification rate in fixed film biofilters. *Aquacultural Engineering, 26*, 221-237.

Zimmerman, R., Richard, D., Lynne, S., & Lin, W. (2005). Is Your MBBR Running on All Cylinders? *Proceedings of the 78th Annual Water Environment Federation Technical Exhibition and Conference.* Washington, DC, Oct. 29 - Nov. 2.

APPENDIX A. MBBR MONITORING AND BENCH TRIALS DATA

Table A.1. Moorhead MBBR biofilm monitoring (Source: Bjornberg, 2009)

Date	Water Temperature (°C)	Attached Biomass (g-TS/m^2)	Volatile Solids (%)	Specific Surface Length (m/m)	Apparent Thickness (µm)
1/11/2007	12.00	12.08			
1/18/2007	10.33	11.97			
1/25/2007	12.67	12.81			
2/1/2007	9.67	13.59			
2/8/2007	9.67	14.72			
2/15/2007	9.33	15.74			
2/22/2007	11.33	14.64			
3/1/2007	11.33	15.29			
3/8/2007	10.67	15.08			
3/15/2007	11.75	14.86			
3/22/2007	11.33	16.04			
3/29/2007	13.30	15.99			
4/5/2007	11.00	16.57			
4/12/2007	12.67	16.82			
4/19/2007	14.00	16.52			
4/26/2007	14.33	18.07			
5/3/2007	14.67	16.72			
5/10/2007	16.00	17.10			
5/17/2007	14.67	15.28			
5/24/2007	15.67	13.87			
5/31/2007	16.50	9.88			
6/7/2007	15.80	9.24			
6/14/2007	17.67	7.40			
6/21/2007	17.00	5.80			
6/28/2007	18.00	5.41			
7/5/2007	19.00	5.29			
7/12/2007	18.33	6.37			
7/19/2007	19.67	6.21			
7/26/2007	20.67	5.53			
8/2/2007	20.67	5.28			
8/9/2007	20.00	5.09			
8/16/2007	20.33	5.04			

Date	Water Temperature (°C)	Attached Biomass (g-TS/m^2)	Volatile Solids (%)	Specific Surface Length (m/m)	Apparent Thickness (µm)
8/23/2007	20.00	5.80			
8/30/2007	20.00	4.51			
9/6/2007	21.00	6.09			
9/13/2007	18.00	5.40			
9/20/2007	19.00	5.38			
9/27/2007	19.00	5.34			
10/4/2007	19.00	4.97			
10/11/2007	16.67	5.60			
10/18/2007	18.33	5.78			
10/25/2007	17.00	6.15			
11/1/2007	17.33	6.13			
11/8/2007	14.33	6.40			
11/15/2007	14.67	6.02			
11/22/2007	14.67	7.20			
11/29/2007	11.33	7.51			
12/6/2007	13.33	7.18			
12/13/2007	12.67	7.49			
12/20/2007	12.67	7.36			
12/27/2007	12.67	7.87			
1/3/2008	10.67	8.35			
1/10/2008	12.33	7.93			
1/17/2008	10.67	8.29			
1/24/2008	10.00	9.32			
1/31/2008	8.67	9.52			
2/7/2008	10.33	9.21			
2/14/2008	9.67	10.07			
2/21/2008	9.00	10.21			
2/28/2008	11.00	11.50			
3/6/2008	9.00	11.01			
3/13/2008	12.00	11.33			
3/20/2008	12.00	12.02			
3/27/2008	11.33	11.88			
4/3/2008	12.00	12.80			
4/10/2008	13.00	12.66			
4/17/2008	13.00	12.49			
4/24/2008	13.67	12.78			

Date	Water Temperature (°C)	Attached Biomass (g-TS/m^2)	Volatile Solids (%)	Specific Surface Length (m/m)	Apparent Thickness (µm)
5/1/2008	12.67				119.39
5/8/2008	14.00	14.84			127.98
5/15/2008	14.00	14.97			155.64
5/22/2008	14.33	15.01			101.83
5/29/2008	15.00	14.43			129.27
6/5/2008	15.00	13.98			102.22
6/12/2008	14.67	13.09		2.46	162.90
6/19/2008	16.00	13.30		2.63	137.33
6/26/2008	17.67	12.01		3.05	147.07
7/3/2008	17.67	10.31		3.06	130.60
7/10/2008	17.67	8.89		2.69	70.98
7/17/2008	18.67	7.65		2.26	49.30
7/24/2008	19.00	7.35		2.14	70.99
7/26/2008	20.00	7.45		2.20	62.90
7/31/2008	19.67	7.56		2.06	66.00
8/7/2008	19.67	6.85		1.80	60.77
8/14/2008	19.33	7.16		2.54	74.90
8/21/2008	20.33	7.50		2.48	53.65
8/28/2008	19.33	7.51	0.451	2.47	68.98
8/30/2008	19.00	7.43		2.10	68.70
9/4/2008	18.80	6.91		2.10	69.21
9/11/2008	18.33	7.23		1.98	60.34
9/18/2008	18.67	7.65	0.403	2.28	80.59
9/25/2008	19.33	7.16	0.346	1.82	74.23
10/2/2008	18.00	7.23	0.282	1.93	49.29
10/9/2008	17.33	7.26	0.431	1.80	57.36
10/11/2008	15.50	7.07		2.40	53.10
10/16/2008	16.00	7.45	0.419	2.43	57.48
10/23/2008	16.33	7.72	0.367	2.45	54.53
10/30/2008	15.00	8.75	0.263	2.81	91.50
11/6/2008	17.33	9.08	0.331	2.51	100.10
11/13/2008	14.67	10.06	0.406	2.69	62.66
11/15/2008	14.50	9.75		2.80	103.20
11/20/2008	12.00	10.30	0.399	2.75	116.84
11/27/2008	13.67	11.19	0.369	3.24	163.89
12/4/2008	11.75	11.58	0.373	3.27	160.52

Date	Water Temperature (°C)	Attached Biomass (g-TS/m^2)	Volatile Solids (%)	Specific Surface Length (m/m)	Apparent Thickness (µm)
12/11/2008	10.00	13.00	0.357		
12/18/2008	8.33	13.54	0.374		
12/25/2008	8.50	14.54	0.494	3.54	151.36
12/27/2008	11.00	14.23	0.445	3.40	153.70
1/1/2009	9.25	13.54			
1/8/2009	10.33	14.54		3.40	172.75
1/15/2009	7.67				
1/22/2009	12.00	16.21		4.09	203.58
1/24/2009	10.00	18.77		3.70	216.30
1/29/2009	10.00				
2/5/2009	12.00	19.04		3.49	284.74

Table A.2. Bench-scale trials 1 and 2 data – 7/26/2008 (Source: Bjornberg, 2009)

	Trial 1 (20°C)		Trial 2 (20°C)	
Time (min)	Ammonia-N (mg/L)	Dissolved Oxygen (mg/L)	Ammonia-N (mg/L)	Dissolved Oxygen (mg/L)
0	31.4	6.5	33.6	7.1
15	30.9	7.8	33.3	8.0
30	29.4	7.9	31.0	8.1
45	27.3	7.9	28.8	7.9
60	25.1	7.9	26.2	8.0
75	22.6	7.8	24.3	7.9
90	20.4	7.8	22.4	8.0
105	18.2	7.9	20.4	8.0
120	16.4	7.9	18.4	7.9
135	15.0	7.8	16.8	8.0
150	13.8	7.9	15.1	8.0
165	12.6	7.9	13.1	8.0
180	11.4	7.8	11.5	7.9
195	10.5	7.8	9.8	7.9
210	9.1	7.8	8.4	8.0
225	6.6	7.8	6.7	7.9
240	5.0	7.8	5.4	7.9
255	3.0	7.9	4.0	8.0
270	2.1	7.8	2.6	8.0
285	1.3	7.9	1.8	8.0
300	0.8	8.0	1.2	8.1
315	0.4	8.3	0.5	8.4
325	0.2	8.5	0.3	8.6
335	0.1	8.6	0.1	8.7

Table A.3. Bench-scale trial 3 data – 8/30/2008 (Source: Bjornberg, 2009)

	Trial 3 (19°C)			
Time (min)	**Ammonia-N (mg/L)**	**Dissolved Oxygen (mg/L)**	**pH (s.u.)**	**Alkalinity (mg/L $CaCO_3$)**
0	25.1	8.5	6.7	300
15	23.2	8.4		
30	21.2	8.3	7.9	283
45	19.0	8.2		
60	17.2	8.1	7.9	250
75	15.0	8.1		
90	12.5	8.1	7.9	217
105	11.0	8.1		
120	8.4	8.2	7.8	200
135	6.7	8.2		
150	5.1	8.2	7.8	167
165	3.6	8.1		
180	1.8	8.1	7.7	133
195	0.8	8.4		
210	0.2	9.3	7.8	117
225	0.1	9.8	7.9	117

Table A.4. Bench-scale trial 4 data – 8/30/2008 (Source: Bjornberg, 2009)

	Trial 4 (19°C)			
Time (min)	**Ammonia-N (mg/L)**	**Dissolved Oxygen (mg/L)**	**pH (s.u.)**	**Alkalinity (mg/L $CaCO_3$)**
0	22.8	8.3	6.8	300
15	20.7	8.3		
30	17.9	8.3	7.9	250
45	15.2	8.3		
60	13.2	8.4	7.9	217
75	11.5	8.3		
90	9.7	8.2	7.9	200
105	7.8	8.3		
120	5.8	8.2	7.8	183
135	4.2	8.2		
150	2.8	8.1	7.8	150
165	1.4	8.2		
180	0.5	8.6	7.8	133
195	0.1	9.3		
210	0.1	9.8	7.9	117

Table A.5. Bench-scale trial 5 data – 10/11/2008 (Source: Bjornberg, 2009)

	Trial 5 (15°C)			
Time (min)	**Ammonia-N (mg/L)**	**Dissolved Oxygen (mg/L)**	**pH (s.u.)**	**Alkalinity (mg/L $CaCO_3$)**
0	12.5	8.8	7.1	300
15	10.2	9.6	7.9	283
30	9.0	9.6		
45	7.8	9.6	8.1	250
60	6.7	9.6		
75	5.7	9.6	8.1	238
90	4.6	9.6		
105	3.7	9.7	8.1	225
120	2.7	9.7		
135	1.7	9.7	8.0	213
150	1.1	9.8		
165	0.5	9.8	8.1	200
180	0.2	9.9		
195	0.1	10.1	8.2	200

Table A.6. Bench-scale trial 6 data – 10/11/2008 (Source: Bjornberg, 2009)

	Trial 6 (16°C)			
Time (min)	**Ammonia-N (mg/L)**	**Dissolved Oxygen (mg/L)**	**pH (s.u.)**	**Alkalinity (mg/L $CaCO_3$)**
0	13.5	9.4	6.9	313
15	11.9	9.8		
30	10.2	9.9	8.0	275
45	8.7	9.9		
60	7.8	9.9	8.1	263
75	6.7	10.0		
90	5.1	10.0	8.1	250
105	4.2	10.0		
120	2.8	10.0	8.2	238
135	1.9	10.0		
150	1.1	10.1	8.1	213
165	0.4	10.2		
180	0.2	10.4	8.3	200

Table A.7. Bench-scale trial 7 data – 11/15/2008 (Source: Bjornberg, 2009)

	Trial 7 (14°C)					
Time (min)	**Ammonia-N (mg/L)**	**Dissolved Oxygen (mg/L)**	**pH (s.u.)**	**Alkalinity (mg/L $CaCO_3$)**	**Nitrite-N (mg/L)**	**Nitrate-N (mg/L)**
0	23.4	8.2	6.9	410	1.4	0.2
15	20.8	8.7				
30	18.2	8.8	8.0	383	1.6	3.2
45	16.3	8.6				
60	14.5	8.3	8.1	350	1.2	6.6
75	12.9	8.1				
90	11.3	7.9	8.1	317	1.5	9.7
105	10.3	7.9				
120	8.4	7.8	8.0	300	1.6	13.2
135	6.1	7.8				
150	4.7	7.8	8.1	283	1.4	17.0
165	3.3	7.8				
180	1.8	7.8	8.0	267	1.5	19.8
195	0.9	7.9				
210	0.3	8.0	8.1	250	1.3	23.4
225	0.1	8.1				

Table A.8. Bench-scale trial 8 data – 11/15/2008 (Source: Bjornberg, 2009)

	Trial 8 (15°C)					
Time (min)	**Ammonia-N (mg/L)**	**Dissolved Oxygen (mg/L)**	**pH (s.u.)**	**Alkalinity (mg/L $CaCO_3$)**	**Nitrite-N (mg/L)**	**Nitrate-N (mg/L)**
0	29.0	7.9	7.1	417	1.3	0.5
15	28.3	8.0				
30	27.1	7.9	8.0	400		
45	24.0	7.8				
60	20.8	7.7	8.1	367	1.6	6.5
75	18.9	7.7				
90	16.8	7.7	8.1	350		
105	15.1	7.7				
120	12.5	7.8	8.1	317	1.5	13.1
135	9.7	7.8				
150	8.1	7.8	8.0	283		
165	5.4	7.7				
180	3.3	7.7	8.1	267	1.5	20.3
195	1.1	7.8				
210	0.4	7.9	8.1	250		
225	0.2	8.0			1.2	22.9

Table A.9. Bench-scale trial 9 data – 12/27/2008 (Source: Bjornberg, 2009)

	Trial 9 (11°C)					
Time (min)	**Ammonia-N (mg/L)**	**Dissolved Oxygen (mg/L)**	**pH (s.u.)**	**Alkalinity (mg/L $CaCO_3$)**	**Nitrite-N (mg/L)**	**Nitrate-N (mg/L)**
0	17.3	8.6	7.1	317	1.3	0.2
15	15.6	8.8				
30	14.2	8.7	7.9	267		
45	12.6	8.8				
60	10.7	8.7	8.0	233	1.5	5.2
75	8.8	8.8				
90	7.5	8.7	8.2	217		
105	5.9	8.7				
120	4.2	8.7	8.0	200	2.0	12.2
135	2.8	8.7				
150	1.3	8.8	7.9	167		
165	0.6	9.4				
180	0.1	9.9	8.1	150	1.2	17.7

Table A.10. Bench-scale trial 10 data – 12/27/2008 (Source: Bjornberg, 2009)

	Trial 10 (11°C)					
Time (min)	**Ammonia-N (mg/L)**	**Dissolved Oxygen (mg/L)**	**pH (s.u.)**	**Alkalinity (mg/L $CaCO_3$)**	**Nitrite-N (mg/L)**	**Nitrate-N (mg/L)**
0	16.7	8.3	7.1	283	0.9	0.1
15	14.8	8.7				
30	13.5	8.7	7.9	267		
45	11.9	8.7				
60	10.1	8.7	8.0	233	1.4	5.7
75	8.6	8.7				
90	7.0	8.6	7.9	217		
105	5.2	8.7				
120	3.7	8.7	7.9	183	1.7	13.3
135	2.3	8.7				
150	0.9	8.9	7.9	167		
165	0.2	9.7				
180	0.1	10.1	8.1	133	0.9	18.3

Table A.11. Bench-scale trial 11 data – 1/24/2009 (Source: Bjornberg, 2009)

	Trial 11 (10°C)					
Time (min)	**Ammonia-N (mg/L)**	**Dissolved Oxygen (mg/L)**	**pH (s.u.)**	**Alkalinity (mg/L $CaCO_3$)**	**Nitrite-N (mg/L)**	**Nitrate-N (mg/L)**
0	34.7	7.1	7.0	317	1.1	0.8
15	32.0	7.0				
30	29.3	6.9	7.9	300		
45	27.0	6.9				
60	25.8	6.8	7.9	267	1.5	5.3
75	23.9	6.8				
90	21.9	6.9	7.9	233		
105	19.4	6.9				
120	17.5	6.8	7.9	217	1.7	12.4
135	15.0	6.8				
150	12.2	6.8	7.8	200		
165	11.1	6.6				
180	9.5	6.5	7.8	167	1.0	17.8
195	7.9	6.4				
210	6.4	6.4	7.8	150		
225	4.9	6.4				
240	3.8	6.3	7.6	117	1.4	21.9
255	2.5	6.3				
270	1.3	6.3	7.6	100		
285	0.6	6.4				
300	0.3	6.4	7.7	83	1.2	32.1

Table A.12. Bench-scale trial 12 data – 1/24/2009 (Source: Bjornberg, 2009)

	Trial 12 (10°C)					
Time (min)	**Ammonia-N (mg/L)**	**Dissolved Oxygen (mg/L)**	**pH (s.u.)**	**Alkalinity (mg/L $CaCO_3$)**	**Nitrite-N (mg/L)**	**Nitrate-N (mg/L)**
0	27.9	6.1	6.7	300	0.9	0.9
15	25.1	6.2				
30	22.5	6.2	7.9	267		
45	20.0	6.1				
60	18.1	6.1	8.0	233		
75	16.4	6.1				
90	14.8	6.0	7.9	200	1.3	8.8
105	13.5	6.0				
120	11.7	6.0	7.9	183		
135	10.1	6.0				
150	8.8	6.0	7.9	167		
165	7.3	6.0				
180	5.9	5.9	7.8	150	1.1	18.2
195	4.4	5.9				
210	3.1	5.9	7.7	133		
225	1.9	5.9				
240	0.9	6.0				
255	0.5	6.0	7.7	83	1.4	25.1

APPENDIX B. CRANK-NICOLSON MODEL DEVELOPMENT

Ammonia-N concentration (N) is a function of position (x) and time (t):

$$N = f(x,t) \tag{B.1}$$

Crank-Nicolson discretization for N, where i represents time and j represents position:

$$N = N_j^i \tag{B.2}$$

System model (from Equations 4.2 and 4.13), where j is equal to 1:

$$V_L \frac{dN}{dt} = -\frac{D_W}{L_L}(N_b - N_s) \times A_b, \qquad (0 \le t, L \le x \le L_L) \tag{B.3}$$

$$V_L \frac{N_b^{i+1} - N_b^i}{\Delta t} = \beta \frac{D_W}{L_L} A_b\left(N_b^i - N_s^i\right) + (1-\beta)\frac{D_W}{L_L} A_b\left(N_b^{i+1} - N_s^{i+1}\right) \tag{B.4}$$

$$k_f = \frac{D_w}{L_L}, \qquad v = \frac{-\Delta t k_f}{V_L}, \qquad \beta = 0.5, \qquad \gamma = 1 - \beta, \qquad b = j, \qquad s = j+1 \tag{B.5}$$

$$\left(1 - \gamma v A_j\right)N_j^{i+1} + \gamma v A_j N_{j+1}^{i+1} = \left(1 + \beta v A_j\right)N_j^i - \beta v A_j N_{j+1}^i \tag{B.6}$$

Biofilm model (from Equations 4.17 and 4.29):

$$A(x)\frac{\partial N}{\partial t} = D_B \frac{\partial}{\partial x}\left(A(x)\frac{\partial N}{\partial x}\right) - A(x)\frac{\mu_m N}{K_N + N}\frac{X}{Y}, \qquad (0 \le t, 0 \le x \le L) \tag{B.7}$$

$$\Delta V \frac{\partial N}{\partial t} = D_B A_{x+\Delta x}\frac{\partial N}{\partial x}\Big|_{x+\Delta x} - D_B A_x \frac{\partial N}{\partial x}\Big|_x - \Delta V \frac{\mu_m N}{K_N + N}\frac{X}{Y} \tag{B.8}$$

$$A_x \Delta x \frac{\partial N}{\partial t} = D_B A_{x-\Delta x/2} \frac{\partial N}{\partial x}\Big|_{x-\Delta x/2} - D_B A_{x+\Delta x/2} \frac{\partial N}{\partial x}\Big|_{x+\Delta x/2} - A_x \Delta x \frac{\mu_m N}{K_N + N} \frac{X}{Y} \tag{B.9}$$

$$\begin{aligned} A_j \frac{N_j^{i+1} - N_j^i}{\Delta t} &= D_B \frac{\beta\left[A_{j+1/2}\left(N_{j+1}^i - N_j^i\right) - A_{j-1/2}\left(N_j^i - N_{j-1}^i\right)\right]}{(\Delta x)^2} \\ &+ D_B \frac{(1-\beta)\left[A_{j+1/2}\left(N_{j+1}^{i+1} - N_j^{i+1}\right) - A_{j-1/2}\left(N_j^{i+1} - N_{j-1}^{i+1}\right)\right]}{(\Delta x)^2} - A_j \frac{\mu_m N_j^i}{K_N + N_j^i} \frac{X}{Y} \end{aligned} \tag{B.10}$$

$$d = \frac{D_B \Delta t}{(\Delta x)^2}, \qquad r = \frac{\mu_m X \Delta t}{Y}, \qquad k = K_s \tag{B.11}$$

$$\begin{aligned} &-d\gamma A_{j-1/2} N_{j-1}^{i+1} + A_j[1 + 2d\gamma] N_j^{i+1} - d\gamma A_{j+1/2} N_{j+1}^{i+1} \\ &= d\beta A_{j-1/2} N_{j-1}^i + A_j[1 - 2d\beta] N_j^i + d\beta A_{j+1/2} N_{j+1}^i - A_j \frac{r N_j^i}{k + N_j^i} \end{aligned} \tag{B.12}$$

Boundary condition 1 (from Equations 4.32 and B.12), where j is equal to j_{max}:

$$-D_B \frac{dN}{dx}\Big|_{x=0} = 0 \tag{B.13}$$

$$\frac{N_{j+1}^{i+1} - N_{j-1}^{i+1}}{2\Delta x} = 0, \qquad \frac{N_{j+1}^i - N_{j-1}^i}{2\Delta x} = 0 \tag{B.14}$$

$$N_{j+1}^{i+1} = N_{j-1}^{i+1}, \qquad N_{j+1}^i = N_{j-1}^i, \qquad A_{j+1/2} = A_j \tag{B.15}$$

$$\begin{aligned} &\left[-d\gamma A_{j-1/2} - d\gamma A_j\right] N_{j-1}^{i+1} + \left[A_j + d\gamma A_j + d\gamma A_{j-1/2}\right] N_j^{i+1} \\ &= \left[d\beta A_{j-1/2} + d\beta A_j\right] N_{j-1}^i + \left[A_j - d\beta A_j - d\beta A_{j-1/2}\right] N_j^i - A_j \frac{r N_j^i}{k + N_j^i} \end{aligned} \tag{B.16}$$

Boundary condition 2 (from Equations 4.34 and B.12), where j is equal to 2:

$$D_B \frac{dN}{dx}\Big|_{x=L} = -\frac{D_W}{L_L}(N_b - N_s) \tag{B.17}$$

$$\begin{aligned} A_j\left(\frac{\Delta x + L_L}{2}\right)\frac{N_j^{i+1} - N_j^i}{\Delta t} &= \beta\left[D_B\frac{A_{j+1/2}\left(N_{j+1}^i - N_j^i\right)}{\Delta x} - D_w\frac{A_j\left(N_j^i - N_{j-1}^i\right)}{L_L}\right] \\ &+(1-\beta)\left[D_B\frac{A_{j+1/2}\left(N_{j+1}^{i+1} - N_j^{i+1}\right)}{\Delta x} - D_w\frac{A_j\left(N_j^{i+1} - N_{j-1}^{i+1}\right)}{L_L}\right] - A_j\frac{\Delta x}{2}\frac{\mu_m N_j^i}{K_s + N_j^i}\frac{X}{Y} \end{aligned} \tag{B.18}$$

$$g = \frac{D_w \Delta t}{L_L}, \qquad h = \frac{D_B \Delta t}{\Delta x}, \qquad p = \frac{\Delta x + L_L}{2}, \qquad w = \frac{\Delta x \Delta t \mu_m X}{2Y} \tag{B.19}$$

$$\begin{aligned} -g\gamma A_j N_{j-1}^{i+1} + \left(h\gamma A_{j+1/2} + g\gamma A_j + A_j p\right)N_j^{i+1} - h\gamma A_{j+1/2}N_{j+1}^{i+1} \\ = g\beta A_j N_{j-1}^i - \left(h\beta A_{j+1/2} + g\beta A_j + A_j p\right)N_j^i + h\beta A_{j+1/2}N_{j+1}^i - A_j\frac{wN_j^i}{k + N_j^i} \end{aligned} \tag{B.20}$$